A STABILIZED FINITE ELEMENT METHOD FOR INCOMPRESSIBLE, INERTIAL FLOWS IN INHOMOGENEOUS POROUS MEDIA

GUILLERMO CASAS*, JOAQUÍN GONZÁLEZ-USÚA†, RAMON CODINA , AND IGNASI DE POUPLANA

Abstract. We present a finite element method for a generalized version of the Navier-Stokes equations that is applicable to (highly permeable) porous media flows. We rely on the variational multiscale (VMS) framework to produce a stabilized numerical method that allows the use of equal-order finite element spaces for all the problem unknowns, while also preventing the instabilities associated to convection-dominated flows or strong reaction terms. Two variants of the basic algorithm are considered and tested in a selection of numerical experiments designed to examine their performance when changing the relative magnitudes of the different terms in the momentum balance equation.

Key words. finite element, stabilized, variational multiscale, VMS, OSGS, generalized Navier-Stokes, Darcy-Brinkman-Forchheimer, particle-laden flows

AMS subject classifications. 65Z05, 65M60, 65N30, 65N12

1. Introduction.

Porous media flows are typically modelled by a pointwise generalization of the classical Darcy equation, which results from postulating that the flow is in a state of permanent local mechanical equilibrium, with the pressure gradient and external body forces balancing the interfacial viscous resistance caused by the fluid's motion relative to the porous matrix. In these conditions, the fluid's inertia, as well as the contribution of the viscous forces arising from the fluid motion relative to itself, can be neglected.

The adequacy of the Darcy model in describing a wide range of porous media flows is empirically well established and has even been rigorously derived in a number of idealized scenarios by applying homogenization theory, with the Stokes equations as a description of the microscopic flow [19, 6]. However, the underlying assumptions of negligible inertia and clear separation of scales fail to hold in a number of practical scenarios encountered in the oil and gas [32, 29], biomedical [27, 17] or food [30] industries, to name but a few. Nonetheless, the application of homogenization theory under relaxed assumptions is still possible, yielding generalized equations that encompass the Darcy equation as a limiting case [7, 5].

Non-Darcy effects can be mathematically captured by incorporating a more sophisticated, nonlinear resistance term into the momentum conservation equation, along with additional terms: the inertia term that stems from taking the material derivative of the flow when describing the local conservation of momentum in an Eulerian framework, and a viscous term (the Brinkman term) representing the intra-fluid viscous forces[1]. As a result, the equations of motion acquire the basic form of the Navier-Stokes equations for incompressible flow (generalized to include a viscous resistance term), with modifications to account for the varying porosity that affect both the momentum and mass conservation equations [3]. A widely used model conforming to the preceding description is that defined by the Darcy-Brinkman-Forchheimer (DBF) equations, applicable to high-permeability, low viscosity flows; see [18] for a

*CIMNE (gcasas@cimne.upc.edu).
†CIMNE (jgonzalez@cimne.upc.edu).

[1] Even though the relevance of this term in particular seems to be very restricted [1]

discussion about the applicability regimes of various porous media flow equations, including DBF.

From the numerical standpoint, the generalized equations bring about all the well-known problems associated with the discretization of the generalized Navier-Stokes system. That is, the Galerkin form of their finite element discretization suffers from instabilities that appear when the viscous term is dominated by any of the lower-order terms such as in convection-dominated or reaction-dominated flows. Furthermore, the use of equal-order interpolations for the velocity and the pressure leads to the violation of the Ladyzhenskaya-Babuška-Brezzi (LBB) condition, requiring stabilization regardless of the situation.

For the Navier-Stokes system, all of these numerical issues have been successfully addressed in the past [10, 11, 16] using the Variational Multi-scale (VMS) framework [21] to design stabilized methods. In [10], the so-called Algebraic Sub-Grid Scale (ASGS) formulation is applied to the Navier-Stokes system, including a reactive term (as well as additional terms related to Coriolis forces which we will not consider here), where optimal error estimates are proven for the linearized problem.

Our goal in this work is to present a numerical method for highly permeable porous media flows. To accomplish this, we generalize the formulation presented in [10], allowing for the presence of an externally-imposed porosity field, and analyze the extent to which the various results obtained in this work carry over to the present setting. Indeed, our analysis shows that essentially the same stability and convergence properties are preserved for the problem analyzed herein if the porosity field is smooth and has bounded gradients that are sufficiently resolved by the mesh. This conclusion is backed up by a battery of numerical tests that explore the robustness of the method with respect to changes in the physical parameters. Over the course of drafting the present paper, we came across the work [22], which applies VMS to the so-called Navier-Stokes-Brinkman system, applicable to highly-permeable porous media flows with a *uniform* porosity field. Except for the presence of a nonlinear reaction term, the theory in [10] fully applies to this case, so no need for revisiting the theory was required there.

The formulation presented here is general enough to encompass alternative variants of the VMS formulation, defined by different choices of the space where the sub-grid scales (SGS) live (see subsection 3.2). This generality can be useful for researchers or engineers looking to explore alternative possibilities to the basic method. In particular, we consider the so-called Orthogonal Sub-Grid Scale (OSGS) [11, 12] alongside the ASGS in all our numerical tests.

Our approach has some advantages over previous efforts that were able to successively address the numerical challenges mentioned above, including the use of inf-sup stable element pairs [8], with the associated complexity increase in the associated data structures required; or the only precedent of a stabilized finite element method: the Local Projection Stabilization [28], which, apart from requiring the use of special enrichment functions, introduces some constraints on the mesh topology.

The rest of the paper is organized as follows. The continuous problem is introduced in section 2. In section 3 we rewrite the strong problem in standard form and apply the VMS approach. In section 4 we provide a rationale behind the design of the unspecified algorithmic parameters. Their design is motivated by an argument based on the Fourier transform that can be found in [11, 26, 13] but that, to our knowledge, had not yet been applied to the Navier-Stokes system in its most recent form. In section 5 the convergence analysis in [10] is extended to the current setting, validating our choice of stabilization parameters. In section 6, we analyze the robust-

ness of the formulation with respect to variations in the physical parameters. Finally, in section 7 we present the results from the numerical experiments, followed by the main conclusions of our work in section 8.

2. The porous Navier-Stokes problem. Let our problem spatial domain be $\Omega \subset \mathbb{R}^d$, with $d \in \{2, 3\}$ its dimension and let $\Gamma := \partial\Omega$ be its boundary. For simplicity, we will consider Ω to be polyhedral. Let $\alpha : \Omega \to (0, 1]$ be a given scalar field over Ω representing the fluid volume fraction. We will assume this field to be differentiable, with a uniformly bounded gradient in Ω. The continuous form of the problem consists in finding (fluid-averaged) pressure and velocity fields, p and $\boldsymbol{u}$, such that

$$\alpha\boldsymbol{u} \cdot \nabla\boldsymbol{u} - 2\nabla \cdot (\alpha\nu \overset{\text{DS}}{\Pi} \nabla\boldsymbol{u}) + \alpha\nabla p + \boldsymbol{\sigma}(\alpha, \boldsymbol{u})\boldsymbol{u} = \boldsymbol{f} \quad \text{in } \Omega, \tag{2.1}$$

$$\varepsilon p + \nabla \cdot (\alpha\boldsymbol{u}) = 0 \quad \text{in } \Omega, \tag{2.2}$$

where $\boldsymbol{\sigma}$ represents a viscous resistance tensor (the inverse of the permeability tensor), which we will assume to be symmetric and positive semidefinite, $\boldsymbol{f}$ is a forcing term representing external body forces, such as gravity, which for simplicity we will assume to be independent of the solution. Finally, $\varepsilon \geqslant 0$ represents a small compressibility, which we mainly include for numerical reasons (i.e., in order to implement the *iterative penalty method* [9]), as in some cases it helps to ensure the well-posedness of the problem; see subsection 7.2.

By defining $\overset{\text{DS}}{\Pi} := \overset{\text{D}}{\Pi}\overset{\text{S}}{\Pi}$, where $\overset{\text{D}}{\Pi}$ and $\overset{\text{S}}{\Pi}$ are (commutative) orthogonal linear projection operators, and considering different versions of the latter two, we obtain alternative formulations found in different contexts in the literature. Our particular choice for these operators in the examples presented, corresponds to taking $\overset{\text{D}}{\Pi}$ and $\overset{\text{S}}{\Pi}$ as the operators that extract, respectively, the deviatoric and symmetric components of the tensor upon which they act. This yields

$$-2\nabla \cdot (\alpha\nu \overset{\text{DS}}{\Pi} \nabla\boldsymbol{u}) = -2\nabla \cdot (\alpha\nu\nabla^{\text{S}}\boldsymbol{u}) + \frac{2}{3}\nabla(\alpha\nu\nabla \cdot \boldsymbol{u}), \tag{2.3}$$

where $\nabla^{\text{S}}\boldsymbol{u} := \frac{1}{2}(\nabla\boldsymbol{u} + (\nabla\boldsymbol{u})^\top)$. This particular formulation for the second term in (2.1) is based on the assumption that the bulk viscosity is zero (Stokes' hypothesis) and it is consistent with the formulation used in multicomponent fluid formulations, where the full system involving several phases is solved in a segregated way, taking one phase at a time and assuming the porosity to be given [24, 23]. Note that for $\alpha \equiv 1$ the incompressible Navier-Stokes system is recovered from (2.1) and (2.2). As mentioned, other combinations are possible. For instance, taking $\overset{\text{D}}{\Pi} \equiv \mathbb{I}$, $\overset{\text{S}}{\Pi} = \nabla^{\text{S}}\boldsymbol{u}$, together with a particular expression for $\boldsymbol{\sigma}$, we recover the DBF equations [8][2]

To complete the definition of the problem, it is necessary to supply the above equations with suitable initial and boundary conditions, whose form will be specified in the following sections. We are not aware of any analysis addressing the well-posedness of resulting problem in its full generality, although in [8] it is proven for the particular case of $\overset{\text{D}}{\Pi} \equiv \mathbb{I}$, $\overset{\text{S}}{\Pi} = \nabla^{\text{S}}\boldsymbol{u}$, a resistance term of the form $\boldsymbol{\sigma} = \sigma(\alpha, \boldsymbol{u})\mathbb{I}$, with σ a scalar function defined in terms of additional scalar functions $a(\alpha), b(\alpha)$ as

$$\sigma(\alpha, \boldsymbol{u}) = a(\alpha) + b(\alpha)|\boldsymbol{u}|, \tag{2.4}$$

[2] Although in other works we find $\overset{\text{D}}{\Pi} = \overset{\text{S}}{\Pi} \equiv \mathbb{I}$ [28], even though the name used for the equations is also DBF.

and a combination of Dirichlet (walls and inlet) and Neumann (outlet) boundary conditions. While we have not attempted a generalization of the results presented in [8], we note that finding an alternative to the explicit use of Korn-type inequalities as done in this work may be nontrivial for $\overset{\mathrm{DS}}{\Pi}=\overset{\mathrm{D\,S}}{\Pi\Pi}$, by which the deviatoric part of the velocity gradient is removed from the viscous term. We will nonetheless proceed by assuming that the solution always exists, and that uniqueness holds for sufficiently large values of ν and of $\inf_\Omega\{\alpha\}$.

2.1. Abstract reformulation of the problem (Strong form). Let $\mathcal{X} := \mathcal{V} \times \mathcal{Q}$ be the space of unknowns, with $\mathcal{V}$ the space of velocity components and $\mathcal{Q}$ that of the pressure; and let $\mathcal{X}'$ be the topological dual of $\mathcal{X}$ (the precise notion of duality to be employed will be determined later). Let us also denote by $n = d + 1$ the number of components of the elements U in $\mathcal{X}$. Consider the following differential operator:

$$\begin{aligned} \mathcal{L}\colon \mathcal{V} \times \mathcal{X} &\to \mathcal{X}' \\ (\boldsymbol{w}, U) &\mapsto \mathcal{L}_{\boldsymbol{w}} U, \end{aligned}$$

where $\mathcal{L}_{\boldsymbol{w}}\colon \mathcal{X} \to \mathcal{X}'$ is a linear differential operator defined by:

$$\mathcal{L}_{\boldsymbol{w}} U = -\partial_i(\mathbf{K}_{ij}\partial_j U) + \mathbf{A}_{\mathrm{c},i}(\boldsymbol{w})\partial_i U + \mathbf{A}_{\mathrm{f},i}\partial_i U + \mathbf{S}(\boldsymbol{w})U. \tag{2.5}$$

In the equations above, the $n \times n$ matrices $\mathbf{K}_{ij}$, $\mathbf{A}_{\mathrm{c},i}(\boldsymbol{w})$, $\mathbf{A}_{\mathrm{f},i}$ and $\mathbf{S}(\boldsymbol{w})$ are either constant or dependent on $\boldsymbol{w}$; i, j run over all the spatial dimensions and ∂_i denotes differentiation with respect to the corresponding spatial coordinate. The usual summation convention for repeated indices is assumed.

Using these definitions, the boundary value problem defined by Equations (2.1) and (2.2), together with appropriate boundary conditions can be cast in the following standard form: *Find* $U = [\boldsymbol{u}; p] \in \mathcal{X}$ *such that*

$$\mathcal{L}_{\boldsymbol{u}} U = F \qquad \text{in } \Omega, \tag{2.6a}$$

$$\mathcal{D}U = \boldsymbol{g} \qquad \text{on } \Gamma, \tag{2.6b}$$

where $F = [\boldsymbol{f}; 0] \in \mathcal{X}'$ and $\boldsymbol{g}$ belonging to the appropriate trace space; with u_i, f_i, g_i $(i = 1 \,..\, d)$ the Cartesian components of $\boldsymbol{u}$ and $\boldsymbol{f}$, and $\boldsymbol{g}$. $\mathcal{D}$ is the trace operator that defines the boundary conditions:

$$\begin{aligned} \mathcal{D}\colon \mathcal{X} &\to L^2(\partial\Omega)^d \\ U &\mapsto \mathcal{D}U =: \mathcal{D}_U, \end{aligned} \tag{2.7}$$

where we have emphasized the linearity of $\mathcal{D}$ (see for example [25]).

The abstract setting above will allow us to directly apply the VMS theory to our particular equations. The specific forms that the different operators take for (2.1) and (2.2) (for $d = 3$) are

$$\mathbf{K}_{ij} = \nu\alpha \begin{bmatrix} \delta_{ij} + \frac{1}{3}\delta_{1i}\delta_{1j} & \delta_{2i}\delta_{1j} - \frac{2}{3}\delta_{1i}\delta_{2j} & \delta_{3i}\delta_{1j} - \frac{2}{3}\delta_{1i}\delta_{3j} & 0 \\ \delta_{1i}\delta_{2j} - \frac{2}{3}\delta_{2i}\delta_{1j} & \delta_{ij} + \frac{1}{3}\delta_{2i}\delta_{2j} & \delta_{3i}\delta_{2j} - \frac{2}{3}\delta_{2i}\delta_{3j} & 0 \\ \delta_{1i}\delta_{3j} - \frac{2}{3}\delta_{3i}\delta_{1j} & \delta_{2i}\delta_{3j} - \frac{2}{3}\delta_{3i}\delta_{2j} & \delta_{ij} + \frac{1}{3}\delta_{3i}\delta_{3j} & 0 \\ 0 & 0 & 0 & 0 \end{bmatrix},$$

(2.8)
$$\mathbf{A}_{\mathrm{c},i}(\boldsymbol{w}) = \alpha \begin{bmatrix} w_i & 0 & 0 & 0 \\ 0 & w_i & 0 & 0 \\ 0 & 0 & w_i & 0 \\ \delta_{i1} & \delta_{i2} & \delta_{i3} & 0 \end{bmatrix}, \mathbf{A}_{\mathrm{f},i} = \alpha \begin{bmatrix} 0 & 0 & 0 & \delta_{i1} \\ 0 & 0 & 0 & \delta_{i2} \\ 0 & 0 & 0 & \delta_{i3} \\ 0 & 0 & 0 & 0 \end{bmatrix},$$
$$\mathbf{S}(\boldsymbol{w}) = \begin{bmatrix} \sigma_{11}(\boldsymbol{w}) & \sigma_{12}(\boldsymbol{w}) & \sigma_{13}(\boldsymbol{w}) & 0 \\ \sigma_{12}(\boldsymbol{w}) & \sigma_{22}(\boldsymbol{w}) & \sigma_{23}(\boldsymbol{w}) & 0 \\ \sigma_{13}(\boldsymbol{w}) & \sigma_{23}(\boldsymbol{w}) & \sigma_{33}(\boldsymbol{w}) & 0 \\ \partial_1\alpha & \partial_2\alpha & \partial_3\alpha & \varepsilon \end{bmatrix},$$

where $\delta_{\bullet\bullet}$ is the Kronecker delta and where in the reaction matrix the dependence of $\boldsymbol{\sigma}$ on α has been (and will henceforth be) omitted for brevity.

The particular version of the trace operator that we will be interested in is given by

(2.9)
$$\begin{aligned} &\mathcal{D}_U \colon \Gamma \to \mathbb{R}^3 \\ &\qquad \boldsymbol{x} \mapsto \begin{cases} \mathcal{D}_{\mathrm{D},U}(\boldsymbol{x}) & \text{if} \quad \boldsymbol{x} \in \Gamma_{\mathrm{D}}, \\ \mathcal{D}_{\mathrm{N},U}(\boldsymbol{x}) & \text{if} \quad \boldsymbol{x} \in \Gamma_{\mathrm{N}}, \end{cases} \end{aligned}$$

where $\Gamma = \Gamma_{\mathrm{D}} \cup \Gamma_{\mathrm{N}}$, $\Gamma_{\mathrm{D}} \cap \Gamma_{\mathrm{N}} = \varnothing$ and where the Dirichlet and Neumann linear operators are defined (for smooth enough fields where the boundary normal $\boldsymbol{n}$ is defined) by

(2.10)
$$\begin{aligned} &\mathcal{D}_{\mathrm{D},U} \colon \Gamma_{\mathrm{D}} \to \mathbb{R}^3 \\ &\qquad \boldsymbol{x} \mapsto \boldsymbol{u}|_\Gamma(\boldsymbol{x}), \end{aligned}$$

(2.11)
$$\begin{aligned} &\mathcal{D}_{\mathrm{N},U} \colon \Gamma_{\mathrm{N}} \to \mathbb{R}^3 \\ &\qquad \boldsymbol{x} \mapsto \alpha\big(\nu \overset{\mathrm{DS}}{\Pi} \nabla \boldsymbol{u}|_\Gamma(\boldsymbol{x}) - p|_\Gamma(\boldsymbol{x})\mathbb{I}\big) \cdot \boldsymbol{n}, \end{aligned}$$

where $|_\Gamma$ denotes the trace of the function on Γ (we may assume α to be defined on the whole of $\partial\Omega$). Moreover, we take

(2.12)
$$\boldsymbol{g}(\boldsymbol{x}) = \begin{cases} \boldsymbol{0} & \text{if } \boldsymbol{x} \in \Gamma_{\mathrm{D}}, \\ \boldsymbol{t}_{\mathrm{N}}(\boldsymbol{x}) & \text{if } \boldsymbol{x} \in \Gamma_{\mathrm{N}}, \end{cases}$$

where $\boldsymbol{t}_{\mathrm{N}}$ is the given traction condition. Thus, note that here we have considered only homogeneous Dirichlet boundary conditions for simplicity, even though all the developments apply equally to the non-homogeneous case, which can be dealt with by applying the standard lifting of the non-homogeneous boundary function to the whole domain.

2.2. Weak form of the problem.

Let us reformulate (2.6) into a form more amenable to the finite element method. We begin by introducing some standard notation. The space of square-integrable functions in a domain ω is denoted as $L^2(\omega)$; the space of functions whose weak derivatives of (integer) order $m \geqslant 0$ and lower belong to $L^2(\omega)$ is denoted by $H^m(\omega)$;

and, for $m = 1$, the subspace of functions in the latter space that additionally fulfill the homogeneous Dirichlet boundary conditions on $\partial\omega$ is denoted $H^1_0(\omega)$. The L^2-inner product in a subdomain $\omega \subseteq \Omega$ is denoted $(\bullet,\bullet)_\omega$ and the integral over ω of the product of two generic functions is written as $\langle \bullet,\bullet \rangle_\omega$, where in both cases the set ω is omitted when $\omega = \Omega$. In particular, the latter notation is used for the pairing between $H^1_0(\omega)$ and its topological dual $H^{-1}(\omega)$. The norm in a space Z is denoted $\|\bullet\|_Z$, except when $Z = L^2(\Omega)$, in which case the subscript is omitted.

Let us now identify the spaces where we will seek the solution to the weak form of the problem. The velocity components will be assumed to belong to $\mathcal{V}_0 \coloneqq H^1_0(\omega)^d$. The pressure will be assumed to belong to $\mathcal{Q}_0 \coloneqq L^2(\Omega)$ in general, while $\mathcal{Q}_0 \coloneqq \{q \in L^2(\Omega) | \int_\Omega q \,\mathrm{d}\Omega = 0\}$ when the boundary conditions in the problem are all-Dirichlet (as with the regular Navier-Stokes system, constraining the solution to this subspace fixes the free constant when $\varepsilon = 0$; for $\varepsilon > 0$ this condition is met automatically).

Using the above notation, the weak form of the problem defined by (2.6) consists in finding $U \in \mathcal{X}_0 \coloneqq \mathcal{V}_0 \times \mathcal{Q}_0$ such that for all $V \in \mathcal{X}_0$,

$$\langle V \,,\, \mathcal{L}U \rangle + \langle V \,,\, \mathcal{D}U \rangle_{\Gamma_\mathrm{N}} = \langle V \,,\, F \rangle + \langle V \,,\, G \rangle_{\Gamma_\mathrm{N}}, \tag{2.13}$$

where $G \coloneqq [\boldsymbol{g}; 0]$. We will assume $\boldsymbol{f} \in \mathcal{V}_0'$ and $\boldsymbol{g} \in H_1^{-1/2}(\Gamma_\mathrm{N})^d$, the latter being the dual of the space of traces on Γ_N of functions in $H^1(\Omega)$. Here and in the sequel we omit the explicit dependence of $\mathcal{L}_{\boldsymbol{u}}$ on $\boldsymbol{u}$ unless we need to emphasize it.

Note that we have not yet specified the space where α, the porosity field, belongs. We will simply assume $\alpha \in W^{1,\infty}(\Omega)$, which ensures that all the terms on the LHS of (2.13) are bounded.

In order to conveniently reexpress this problem in terms of linear functionals, let us introduce the form $B\colon \mathcal{V} \times \mathcal{X} \times \mathcal{X} \to \mathbb{R}$, bilinear with respect to the second and third arguments:

$$\begin{aligned} B(\boldsymbol{w}, U, V) \coloneqq{}& \langle \partial_i V \,,\, \mathbf{K}_{ij} \partial_j U \rangle + \langle V \,,\, \mathbf{A}_{\mathrm{c},i}(\boldsymbol{w}) \partial_i U \rangle \\ & - \langle \partial_i (\mathbf{A}_{f,i}^\top V) \,,\, U \rangle + \langle V \,,\, \mathbf{S}(\boldsymbol{w}) U \rangle, \end{aligned} \tag{2.14}$$

and the linear form $L\colon \mathcal{X} \to \mathbb{R}$, defined as

$$L(V) \coloneqq \langle V \,,\, F \rangle + \langle V \,,\, G \rangle_{\Gamma_\mathrm{N}}. \tag{2.15}$$

Using (2.9), (2.11), (2.14), and (2.15), the weak form of the problem can be reexpressed in terms of the linear forms as follows: *Find* $U = [\boldsymbol{u}; p] \in \mathcal{X}_0$, *such that*

$$B(\boldsymbol{u}, U, V) = L(V) \quad \forall V \in \mathcal{X}_0. \tag{2.16}$$

3. Variational multiscale approach.

We are now ready to apply the VMS framework to derive a stabilized finite element formulation. Thanks to the abstract formulation introduced in the previous section, we can do this systematically, directly following the most general description of the method [15]. In fact, we have chosen to repeat some nonessential parts of the methodology here for the sake of notational conformity and ease of comprehension.

3.1. Scale Splitting.

Let us consider generic finite-dimensional subspaces $\mathcal{X}_{h0} \coloneqq \mathcal{V}_{h0} \times \mathcal{Q}_{h0} \subset \mathcal{X}_0$ and the space $\widetilde{\mathcal{X}}_0$ such that

$$\mathcal{X}_0 = \mathcal{X}_{h0} \oplus \widetilde{\mathcal{X}}_0, \tag{3.1}$$

so that $U = U_h + \widetilde{U}$ (with $U_h \in \mathcal{X}_{h0}$ and $\widetilde{U} \in \widetilde{\mathcal{X}}_0$). Equation (2.13) can now be equivalently written as the following system:

$$\langle V_h \, , \mathcal{L}(U_h + \widetilde{U}) \rangle + \langle V_h \, , \mathcal{D}(U_h + \widetilde{U}) \rangle_{\Gamma_N} = \langle V_h \, , F \rangle + \langle V_h \, , G \rangle_{\Gamma_N} \quad \forall V_h \in \mathcal{X}_{h0}, \tag{3.2}$$

$$\langle \widetilde{V} \, , \mathcal{L}(U_h + \widetilde{U}) \rangle + \langle \widetilde{V} \, , \mathcal{D}(U_h + \widetilde{U}) \rangle_{\Gamma_N} = \langle \widetilde{V} \, , F \rangle + \langle \widetilde{V} \, , G \rangle_{\Gamma_N} \quad \forall \widetilde{V} \in \widetilde{\mathcal{X}}_0. \tag{3.3}$$

Or, in terms of bilinear forms,

$$B(\boldsymbol{u}, U_h, V_h) + B(\boldsymbol{u}, \widetilde{U}, V_h) = L(V_h) \quad \forall V_h \in \mathcal{X}_{h0}, \tag{3.4}$$

$$B(\boldsymbol{u}, U_h, \widetilde{V}) + B(\boldsymbol{u}, \widetilde{U}, \widetilde{V}) = L(\widetilde{V}) \quad \forall \widetilde{V} \in \widetilde{\mathcal{X}}_0. \tag{3.5}$$

Equations (3.4) and (3.5) are the starting point of the VMS methodology. Equation (3.5) will be used to derive an approximation to the SGSs, while (3.4) will become the modified weak form of the problem once the approximate SGSs are introduced in the second term of its left-hand side.

To clarify the motivation behind the scale-splitting strategy, let us note that it is possible to formally eliminate $\widetilde{U}$ from the equations above to obtain

$$B(\boldsymbol{u}, U_h, V_h) - \langle \mathcal{L}\widetilde{\mathcal{L}}^{-1}\mathcal{R}U_h \, , V_h \rangle = L(V_h) \quad \forall V_h \in \mathcal{X}_{h0}, \tag{3.6}$$

where $\mathcal{R}$ is the residual operator, i.e., $\mathcal{R}_{\boldsymbol{w}} \coloneqq F - \mathcal{L}_{\boldsymbol{w}}U$, whose explicit dependence on $\boldsymbol{w}$ we will also omit when $\boldsymbol{w} = \boldsymbol{u}$ (except where emphasis is required), and $\widetilde{\mathcal{L}}^{-1}$ is the fine-scale Green's operator, which gives $\widetilde{U}$ from the coarse-scale residual, i.e., $\widetilde{U} = \widetilde{\mathcal{L}}_U^{-1}(\mathcal{R}U_h)$. Its expression can, in fact, be calculated explicitly [20]:

$$\widetilde{\mathcal{L}}^{-1} = \mathcal{L}^{-1} - \mathcal{L}^{-1}\Pi_h^\top \left(\Pi_h \mathcal{L}^{-1} \Pi_h^\top\right)^{-1} \Pi_h \mathcal{L}^{-1}, \tag{3.7}$$

where Π_h is a linear projection onto $\mathcal{X}_{h0}$ and $\Pi_h^\top$ its transpose. Equation (3.6) is exact and (assuming the continuous problem is well posed) the second term must be providing the desired stability that the first term alone (i.e., the Galerkin method) lacks. Moreover, note that the equation that we obtain by substituting (3.7) in (3.6) is entirely in terms of $\mathcal{L}^{-1}$ and Π_h. Accordingly, all VMS-stabilized methods are characterized by the way in which these two operators are approximated. The idea is always to obtain a computable numerical method, while *still preserving the desired stability properties of the original equation*. In the following subsection, we describe the particular choices made here in order to achieve this.

3.2. Finite element discretization & modelling of SGSs.

The standard Galerkin finite element method consists in replacing the infinite-dimensional space $\mathcal{X}$ by a finite-dimensional analogue, leading to a problem that is finite dimensional and therefore computable. Thus, let us consider a finite element discretization $\bigcup_{K \in \mathcal{T}_h} K = \bar{\Omega}$ (the closure of Ω), constructed with a mesh of diameter h. Let us denote the velocity and pressure finite element spaces as $\mathcal{V}_{h0} \subset \mathcal{V}_0$, and $\mathcal{Q}_{h0} \subset \mathcal{Q}_0$ with $\mathcal{X}_{h0} \coloneqq \mathcal{V}_{h0} \times \mathcal{Q}_{h0}$ and the finite element functions $U_h = [u_{h,1}, \ldots, u_{h,d}, p_h] \in \mathcal{X}_{h0}$ (identifying $[[\bullet_1 \cdots \bullet_d], \bullet]$ with $[\bullet_1 \cdots \bullet_{d+1}]$). To simplify the exposition, we will consider that $\mathcal{V}_{h0}$ and $\mathcal{Q}_{h0}$ are constructed using continuous polynomial interpolations.

As mentioned in the introduction, the discretized problem obtained with the Galerkin method will suffer from numerical instabilities due to the violation of the LBB condition (e.g., for equal-order spaces) and from the degeneration of its inherent stability for extreme values of the physical parameters. Let us therefore use the VMS framework to produce a stabilized formulation of the discrete problem. Considering

the finite element spaces defined by the discretization above in (3.4) and applying Stokes' theorem to each element domain (which, in particular, is possible for piecewise polynomials), we obtain

$$B(\boldsymbol{u}, U_h, V_h) + \sum_K \Big[\langle \mathcal{L}^* V_h \, , \widetilde{U} \rangle_K + \langle \mathcal{D}_{\mathrm{N}}^* V_h \, , \mathcal{D}_K \widetilde{U} \rangle_{\partial K} \Big] = L(V_h) \quad \forall V_h \in \mathcal{X}_{h0} \tag{3.8}$$

with

$$\mathcal{D}_{\mathrm{N}}^* V = n_i \mathbf{K}_{ji}^\top \partial_j V + n_i \mathbf{A}_{\mathrm{c},i}^\top(\boldsymbol{w}) V, \tag{3.9}$$

$$\mathcal{L}^* V = -\partial_i(\mathbf{K}_{ji}^\top \partial_j V) - \partial_i(\mathbf{A}_{c,i}^\top(\boldsymbol{w}) V) - \partial_i(\mathbf{A}_{f,i}^\top V) + \mathbf{S}^\top(\boldsymbol{w}) V, \tag{3.10}$$

and where the asterisks denote duality with respect to the pairing; $\widetilde{U}$ represents an approximation to the SGS that must be provided in terms of the finite element solution; and $\mathcal{D}_K$ is the trace operator that sends sufficiently smooth functions in the interior of K to their evaluation on the boundary ∂K ($\mathcal{D}_K U := U|_{\partial K}$). Note that we omit the subscript of $\mathcal{L}_{\boldsymbol{u}}^*$ for brevity, just as we have done with $\mathcal{L}_{\boldsymbol{u}}$ and $\mathcal{R}_{\boldsymbol{u}}$.

In order to produce an algorithm for the computation of $\widetilde{U}$, one must make certain approximations. There are many options, each defining a particular VMS method [15]. Here we will proceed conventionally, adopting the following assumptions:

- A.1 $\mathcal{D}_K \widetilde{U} = 0$; as a consequence, $\widetilde{\mathcal{X}} = \widetilde{\mathcal{X}}_0$ and thus we assume that the finite element functions are able to resolve the boundary conditions *exactly*.
- A.2 The SGSs are functions of rapid decay, in such a way that their contribution at the element at the inter-element boundaries can be neglected.
- A.3 $\mathcal{L}_{\boldsymbol{u}}^{-1}\big|_K \approx \boldsymbol{\tau}_K(\boldsymbol{u})$; that is, that the inverse of the differential operator of the strong problem restricted to the finite element K can be approximated by $\boldsymbol{\tau}_K$, the matrix of stabilization parameters, which inherits from $\mathcal{L}_{\boldsymbol{u}}^{-1}$ its dependence on $\boldsymbol{u}$ and whose definition will be discussed later.

Note that it is only after these approximations are made, that problem ceases to be equivalent to the original one. In spite of this, we will be keeping the same symbols for the finite element component of the solution, U_h, for the SGS component, $\widetilde{U}$, and for the *total* solution $U = U_h + \widetilde{U}$ from this point on, so it is important to bear in mind the abuse of notation involved.

Using (2.14) and (2.15) and Assumptions A.1 and A.2, (3.3) can be rewritten as

$$\langle \widetilde{V} \, , \mathcal{L}\widetilde{U} \rangle = \langle \widetilde{V} \, , F - \mathcal{L} U_h \rangle \quad \forall \widetilde{V} \in \widetilde{\mathcal{X}} \tag{3.11}$$

or, in terms of the residual operator,

$$\widetilde{\Pi}[\mathcal{L}\widetilde{U}] = \widetilde{\Pi}[\mathcal{R} U_h], \tag{3.12}$$

where $\widetilde{\Pi}$ a projection operator onto the space of SGSs $\widetilde{\mathcal{X}}$.

Using Assumption A.3, this equation can be approximated, within any element domain K, by [15]

$$\begin{aligned} \widetilde{\Pi}[\mathcal{R}_U U_h] \,|_K = \widetilde{\Pi}[\mathcal{L}_{\boldsymbol{u}} \widetilde{U}]|_K \approx \widetilde{\Pi}[\boldsymbol{\tau}_K^{-1}(\boldsymbol{u}) \widetilde{U}]|_K = \boldsymbol{\tau}_K^{-1}(\boldsymbol{u}) \widetilde{U}|_K \\ \implies \widetilde{U}|_K = \boldsymbol{\tau}_K(\boldsymbol{u}) \widetilde{\Pi}[\mathcal{R} U_h] \,|_K \, . \end{aligned} \tag{3.13}$$

Note that (3.13) is nonlinear, due to the dependence of both $\boldsymbol{\tau}_K$ and $\mathcal{R} U_h \,|_K$ on the SGS. Thus, it will be necessary to linearize it at each integration point to obtain a solution in the final formulation; see subsection 3.3.

Summarizing, under A.1 to A.3, (3.8) can be written as the following stabilized system:

$$B(\boldsymbol{u}, U_h, V_h) + \sum_K \langle \mathcal{L}^* V_h \, , \boldsymbol{\tau}_K(\boldsymbol{u}) \widetilde{\Pi}[\mathcal{R}U_h] \rangle_K = L(V_h). \tag{3.14}$$

Different VMS methods are obtained by different choices of the SGSs space. Here we will consider the following methods:

- The ASGS method, where $\widetilde{\mathcal{X}}$ is taken as the space of finite element residuals, and thus $\widetilde{\Pi} = \mathcal{I}$.
- The OSGS method, where $\widetilde{\mathcal{X}}$ is taken as $\mathcal{X}_{h0}^{\perp}$.

The projection operator for the OSGS method is

$$\widetilde{\Pi} = \mathcal{I} - \Pi_{\boldsymbol{\tau} h}, \tag{3.15}$$

where $\Pi_{\boldsymbol{\tau} h}$ is the projection onto $\mathcal{X}_{h0}$ associated to associated to the inner product defined as

$$(\bullet,\bullet)_{\boldsymbol{\tau}} := \sum_K \langle \boldsymbol{\tau}_K \bullet, \bullet \rangle_K. \tag{3.16}$$

In practice, it is often convenient to make the further simplification:

$$(\bullet,\bullet)_{\boldsymbol{\tau}} \approx \sum_K \langle \bullet, \bullet \rangle_K, \tag{3.17}$$

with the corresponding effect on the computation of $\Pi_{\boldsymbol{\tau} h}$. This simplified projection corresponds to the standard L^2-projection, which can be computed very efficiently and has similar stabilizing properties [11].

Taking this approach, and using (3.15) in (3.14), we obtain the following stabilized formulation of the discrete problem: *Find* $U_h \in \mathcal{X}_{h0}$ *such that for all* $V_h \in \mathcal{X}_{h0}$ *and all* $W_h \in \mathcal{X}_{h0}$,

$$B_{\mathrm{S}}(\boldsymbol{u}, U_h, V_h) = L_{\mathrm{S}}(\boldsymbol{u}, V_h, \boldsymbol{\pi}_h), \tag{3.18a}$$

$$\widetilde{U}|_K = \boldsymbol{\tau}_K(\boldsymbol{u}) \, (\mathcal{R}U_h - \boldsymbol{\pi}_h)|_K \quad \forall K \in \mathcal{T}_h, \tag{3.18b}$$

$$\langle W_h \, , \boldsymbol{\pi}_h \rangle = \langle W_h \, , \mathcal{R}U_h \rangle, \tag{3.18c}$$

$$U = U_h + \widetilde{U}, \tag{3.18d}$$

where

$$B_{\mathrm{S}}(\boldsymbol{w}, U, V) := B(\boldsymbol{u}, U, V) - \sum_K \langle \mathcal{L}_{\boldsymbol{w}}^* V \, , \boldsymbol{\tau}_K(\boldsymbol{w}) \mathcal{L}_{\boldsymbol{w}} U \rangle, \tag{3.19}$$

$$L_{\mathrm{S}}(\boldsymbol{w}, V, \boldsymbol{\pi}) := L(V) - \sum_K \langle \mathcal{L}_{\boldsymbol{w}}^* V \, , \boldsymbol{\tau}_K(\boldsymbol{w}) \, (F - \boldsymbol{\pi}) \rangle_K. \tag{3.20}$$

Equation (3.18) is the complete discretized system of equations to be solved corresponding to the OSGS method. The ASGS method is then recovered by simply taking $\boldsymbol{\pi}_h = \mathbf{0}$. This system is nonlinear and of a larger size (in the OSGS case) than the original Galerkin system due to the introduction of the residual projections $\boldsymbol{\pi}_h$. In subsection 3.3 we describe the particular way in which we have decoupled and linearized the system.

3.3. Linearization of the coupled system of discrete equations.

The process of approximating (3.18) to make it numerically tractable involves both its linearization with respect to U, and the decoupling of (3.18a)–(3.18d). To the latter end, note that, while equations (3.18a) and (3.18c) involve the resolution of two global systems, and must therefore be solved separately, (3.18b) and (3.18d) are local, in the sense that they express elemental equations, only involving a reduced number of unknowns. Therefore, it is possible to consider the latter two equations both separately or as a single (monolithic) system to be solved independently on each element without running into unacceptable numerical costs.

Here we have opted for the following iteration scheme for (3.18):

$$B_{\mathrm{S}}(\boldsymbol{u}^{m-1}, U_h^m, V_h) = L_{\mathrm{S}}(\boldsymbol{u}^{m-1}, V_h, \boldsymbol{\pi}_h^m), \tag{3.21a}$$

$$\widetilde{U}^m|_K = \boldsymbol{\tau}_K(\boldsymbol{u}^{m-1})\ (\mathcal{R}_{\boldsymbol{u}^{m-1}} U_h^m - \boldsymbol{\pi}_h^m)|_K\,, \tag{3.21b}$$

$$\langle W_h\,, \boldsymbol{\pi}_h^m \rangle = \langle W_h\,, \mathcal{R}_{\boldsymbol{u}^{m-1}} U_h^{m-1} \rangle, \tag{3.21c}$$

$$U^m = U_h^m + \widetilde{U}^m, \tag{3.21d}$$

where m is the iteration counter. Such iteration can be used to solve the system of equations as shown in Algorithm 3.1.

In all rigor, we should point out that in the implementation of Algorithm 3.1 we do not include the reaction terms in the calculation of the orthogonal projection. The reason is that these terms belong to the finite element space where the solution lives, and so their projection is exactly zero (for constant $\boldsymbol{\sigma}$). However, note that $\boldsymbol{\pi}_h^m$ is calculated with an outdated value of the unknown when one is performing the projections, within the nonlinear iterations loop, using (3.21c). So, were we to include these terms in (3.21c), the projection of the reaction terms would not exactly cancel. Following standard practice, we have modified the algorithm slightly by removing these terms altogether, which is equivalent to considering that their projection is evaluated at the next (still to be reached) iteration step in (3.21a), as the resulting algorithm has been observed to facilitate the convergence of the nonlinear iterations. We have chosen not to include this in Algorithm 3.1 for the sake of generality.

Algorithm 3.1 Solving the nonlinear problem

$m \leftarrow 0$
U_h^m, $\widetilde{U}^m \leftarrow$ `SetInitialGuesses`()
$U^m \leftarrow U_h^m + \widetilde{U}^m$
while `NotConverged`() **do**
  $m \leftarrow m + 1$
  $\boldsymbol{\pi}_h^m \leftarrow$ `ProjectResidual`(U^{m-1}, U_h^{m-1}) ▷ Solve (3.21c)
  $U_h^m \leftarrow$ `SolveGlobalSystem`$(U^{m-1}, \boldsymbol{\pi}_h^m)$ ▷ Solve (3.21a)
  for $K \in \mathcal{T}_h$ **do**
    $\widetilde{U}^m|_K \leftarrow$ `CalculateSubscales`$(U^{m-1}, U_h^m, \boldsymbol{\pi}_h^m)$ ▷ Solve (3.21b)
  end
  $U^m \leftarrow U_h^m + \widetilde{U}^m$ ▷ (3.21d)
end
$U_h^\infty \leftarrow U_h^m$ ▷ Set converged solution

4. Design of the stabilization parameters: Fourier analysis.

In section 3, we have used (3.12) to propose a computable approximation to (3.7)

that can be introduced in (3.4) to define the (stabilized) discrete problem. The basic assumption is that, if this approximation is reasonable, the finite element solution of this problem should be closer to the component of the solution of the continuous problem contained in the finite element space than the Galerkin approximation is. The hope is that this improvement results in a stable method.

Since the matrix of stabilized parameters $\boldsymbol{\tau}_K$ is the only part of the formulation that remains undetermined, our task now reduces to finding suitable approximations for each of its entries (i.e., the stabilization parameters). We will show in this section how the expressions for the stabilization parameters that work for the incompressible Navier-Stokes system can be generalized to the equations we are interested in, preserving the stability of the discrete system.

To achieve this, it is clear that we must somehow relate $\boldsymbol{\tau}_K$ to the original differential operators that define the problem at hand which it purports to approximate. In order to do so, we rely on a heuristic argument based on comparing the norms of $\boldsymbol{\tau}_K$ to that of the Fourier-transformed versions of the original operators. This approach was first published in [11] for the incompressible Navier-Stokes equations and later applied and further developed to several other systems [12, 2, 26].

We begin by defining suitable inner products in the space of forcing terms, $\mathcal{X}'$:

$$(F\,,G)_\Lambda = F^\dagger \Lambda G, \tag{4.1}$$

where the $\dagger$ symbol indicates the conjugate transpose and where Λ is a positive definite matrix that is introduced to make the inner product dimensionally well-defined. It is enough to take (for $d = 3$)

$$\Lambda = \begin{bmatrix} 1 & 0 & 0 & 0 \\ 0 & 1 & 0 & 0 \\ 0 & 0 & 1 & 0 \\ 0 & 0 & 0 & \lambda \end{bmatrix}, \tag{4.2}$$

where λ is a scaling factor with units of velocity squared, to achieve this. Its particular definition will be given later. This inner product defines the norm $|\bullet|_\Lambda := (\bullet\,,\bullet)_\Lambda^{1/2}$. It is straightforward to check that the inner product $(\bullet\,,\bullet)_{\Lambda^{-1}}$ in $\mathcal{X}$ (with its associated norm $|\bullet|_{\Lambda^{-1}}$) is also dimensionally consistent. Finally, we may define the functional norm

$$\|\bullet\|_{L^2_\Lambda(K)} := \left(\int_K |\bullet|_\Lambda^2 \,\mathrm{d}\Omega\right)^{1/2}, \tag{4.3}$$

with $\|\bullet\|_{L^2_{\Lambda^{-1}}(K)}$ defined analogously.

The argument to *motivate* the design of the stabilization parameters, adapted from [12] (see also [26]), goes as follows. There holds

$$\begin{aligned} \|\widetilde{\Pi}[\mathcal{L}\widetilde{U}]\|^2_{L^2_\Lambda(K)} &\approx \|\widetilde{\Pi}[\mathcal{L}\widetilde{U}]\|^2_{L^2_\Lambda(\mathbb{R}^d)} = \|\widehat{\widetilde{\Pi}[\mathcal{L}\widetilde{U}]}\|^2_{L^2_\Lambda(\mathbb{R}^d)} = \int_{\mathbb{R}^d} |\widehat{\mathcal{L}}\widehat{\widetilde{U}}|^2_\Lambda \,\mathrm{d}\boldsymbol{k} \\ &\leqslant \int_{\mathbb{R}^d} |\widehat{\mathcal{L}}|^2_\Lambda |\widehat{\widetilde{U}}|^2_{\Lambda^{-1}} \,\mathrm{d}\boldsymbol{k} = |\widehat{\mathcal{L}}(\boldsymbol{k}_0)|^2_\Lambda \|\widetilde{U}\|^2_{L^2_{\Lambda^{-1}}(\mathbb{R}^d)} \approx |\widehat{\mathcal{L}}(\boldsymbol{k}_0)|^2_\Lambda \|\widetilde{U}\|^2_{L^2_{\Lambda^{-1}}(K)}, \end{aligned} \tag{4.4}$$

where $\boldsymbol{k}$ is the dimensionless h-normalized wave number. The first (strict) equality stems from Plancherel's theorem, while the approximations in the first and second line are the result of neglecting the value of the SGSs (and of their derivatives) on the

element boundary (cf. Assumption A.2). The first equality in the second line is due to the mean value theorem, which predicts the existence of a $\boldsymbol{k}_0$ which, assuming the SGSs are dominated by large wave numbers, must be $|\boldsymbol{k}_0| \gtrsim 1$.

So, if we are to approximate $\mathcal{L}^{-1}$ on each element K by a matrix $\boldsymbol{\tau}_K$, a possible design restriction could be that the approximate version of the inequality in (4.4) holds. This is automatically achieved if one imposes that

$$|\boldsymbol{\tau}_K^{-1}|_\Lambda^2 \leqslant |\widehat{\mathcal{L}}(\boldsymbol{k}_0)|_\Lambda^2. \tag{4.5}$$

In particular, we take $\boldsymbol{\tau}_K$ so that the equality holds. A convenient way to impose such condition is to consider the set of eigenvalues of the generalized eigenvalue problem given, for any matrix $\mathbf{A}$, by $\mathrm{spec}_{\Lambda^{-1}}(\mathbf{A}) = \left\{\lambda : \mathbf{A}\boldsymbol{x} = \lambda\Lambda^{-1}\boldsymbol{x}\right\}$. It can be shown that (4.5) can be achieved by imposing that the spectral radius of $\boldsymbol{\tau}_K^{-1}\Lambda\boldsymbol{\tau}_K^{-1}$ be equal to that of $\widehat{\mathcal{L}}^\dagger(\boldsymbol{k}_0)\Lambda\widehat{\mathcal{L}}(\boldsymbol{k}_0)$, where the definition of spectral radius in this context is given by $\rho_{\Lambda^{-1}}(\mathbf{A}) \coloneqq \max\left(\mathrm{spec}_{\Lambda^{-1}}(\mathbf{A})\right)$.

Now comes a step that is not completely systematic: we are looking for a decomposition of the differential operator in (2.5) that leads to a simplified version of (4.5). This decomposition is not unique and may require a few iterations, even though it can be motivated by previous similar decompositions and the physics of the problem (decompose the matrices into similar physical effects). Here we propose the following:

$$\mathcal{L}W = \left(\mathcal{L}_\nu + \mathcal{L}_c + \mathcal{L}_b + \mathcal{L}_\sigma + \mathcal{L}_{\nabla\alpha}\right)W, \tag{4.6}$$

with

$$\mathcal{L}_\nu W \coloneqq -\partial_i(\mathbf{K}_{ij}\partial_j W), \tag{4.7}$$

$$\mathcal{L}_c W \coloneqq \mathbf{A}_{v,i}\partial_i W, \tag{4.8}$$

$$\mathcal{L}_b W \coloneqq \mathbf{A}_{b,i}\partial_i W, \tag{4.9}$$

$$\mathcal{L}_\sigma W \coloneqq \mathbf{S}_\sigma W, \tag{4.10}$$

$$\mathcal{L}_{\nabla\alpha} W \coloneqq \mathbf{S}_{\nabla\alpha} W, \tag{4.11}$$

where

$$\mathbf{A}_{v,i}(\boldsymbol{w}) = \alpha \begin{bmatrix} w_i & 0 & 0 & 0 \\ 0 & w_i & 0 & 0 \\ 0 & 0 & w_i & 0 \\ 0 & 0 & 0 & 0 \end{bmatrix}, \ \mathbf{A}_{b,i} = \alpha \begin{bmatrix} 0 & 0 & 0 & \delta_{i1} \\ 0 & 0 & 0 & \delta_{i2} \\ 0 & 0 & 0 & \delta_{i3} \\ \delta_{i1} & \delta_{i2} & \delta_{i3} & 0 \end{bmatrix} \tag{4.12}$$

$$\mathbf{S}_{\nabla\alpha} = \begin{bmatrix} 0 & 0 & 0 & 0 \\ 0 & 0 & 0 & 0 \\ 0 & 0 & 0 & 0 \\ \partial_1\alpha & \partial_2\alpha & \partial_3\alpha & 0 \end{bmatrix}, \tag{4.13}$$

and where $\mathbf{S}_\sigma = \mathbf{S} - \mathbf{S}_{\nabla\alpha}$. Note that different physical parameters appear in different operators and that different-order derivatives do as well.

Now, due to the complexity of the operator $\mathcal{L}$, instead of (4.5), we will consider

$$\boldsymbol{\tau}_K^{-1} = \boldsymbol{\tau}_\nu^{-1} + \boldsymbol{\tau}_c^{-1} + \boldsymbol{\tau}_b^{-1} + \boldsymbol{\tau}_\sigma^{-1} + \boldsymbol{\tau}_{\nabla\alpha}^{-1}. \tag{4.14}$$

For simplicity, we take $\boldsymbol{\tau}_K = \mathrm{diag}\left(\tau_1, \tau_1, \tau_1, \tau_2\right)$ (for $d = 3$) and every matrix on the right-hand side of (4.14) is taken of the same form. Every approximate operator is thus defined by a pair of (positive) eigenvalues, whose value is fixed by the following

design criterion: their value should be taken as the minimum still ensuring that the spectral radius of the approximate operator is as large as that of its corresponding Fourier-transformed differential operator, and such that the kernel of the former is contained in that of the latter. Note that this condition guarantees that

$$|\boldsymbol{\tau}_K^{-1}|_\Lambda^2 \leqslant |\boldsymbol{\tau}_\nu^{-1}|_\Lambda^2 + |\boldsymbol{\tau}_c^{-1}|_\Lambda^2 + |\boldsymbol{\tau}_b^{-1}|_\Lambda^2 + |\boldsymbol{\tau}_\sigma^{-1}|_\Lambda^2 + |\boldsymbol{\tau}_{\nabla\alpha}^{-1}|_\Lambda^2 \tag{4.15}$$

$$= |\widehat{\mathcal{L}}_\nu(\boldsymbol{k}_0)|_\Lambda^2 + |\widehat{\mathcal{L}}_c(\boldsymbol{k}_0)|_\Lambda^2 + |\widehat{\mathcal{L}}_b(\boldsymbol{k}_0)|_\Lambda^2 + |\widehat{\mathcal{L}}_\sigma(\boldsymbol{k}_0)|_\Lambda^2 + |\widehat{\mathcal{L}}_{\nabla\alpha}(\boldsymbol{k}_0)|_\Lambda^2 \tag{4.16}$$

which, while not strictly implying (4.5), reduces to it in the limit when any of the operators becomes dominant. The same design criterion has been successfully applied to other problems [26]. The expression of the Fourier-transformed operators is (summation over repeated indices is implied)

$$\widehat{\mathcal{L}}_\nu(\boldsymbol{k}_0) \approx \frac{k_{0,i}k_{0,j}}{h^2}\mathbf{K}_{ij}, \tag{4.17}$$

$$\widehat{\mathcal{L}}_c(\boldsymbol{k}_0) \approx \mathrm{i}\frac{k_{0,i}}{h}\mathbf{A}_{v,i}, \tag{4.18}$$

$$\widehat{\mathcal{L}}_b(\boldsymbol{k}_0) \approx \mathrm{i}\frac{k_{0,i}}{h}\mathbf{A}_{b,i}, \tag{4.19}$$

$$\widehat{\mathcal{L}}_\sigma(\boldsymbol{k}_0) \approx \mathbf{S}_\sigma, \tag{4.20}$$

$$\widehat{\mathcal{L}}_\sigma(\boldsymbol{k}_0) \approx \mathbf{S}_{\nabla\alpha}, \tag{4.21}$$

where i denotes the imaginary unit and where we have used the fact that the fluid volume fraction field α (and likewise $\nabla\alpha$) is slowly varying compared to the SGSs, so it may be taken as a constant in the Fourier transform.

Using these definitions and applying the design criteria above yields the following stabilization parameters:

$$\begin{aligned}
\tau_{\nu,1}^{-1} &= \frac{4}{3}\alpha\nu\frac{|\boldsymbol{k}_0|}{h^2}, & \tau_{\nu,2}^{-1} &= 0,\\
\tau_{c,1}^{-1} &= \alpha\frac{\boldsymbol{w}\cdot\boldsymbol{k}_0}{h}, & \tau_{c,2}^{-1} &= 0,\\
\tau_{b,1}^{-1} &= \alpha\frac{|\boldsymbol{k}_0|}{h}\sqrt{\lambda}, & \tau_{b,2}^{-1} &= \alpha\frac{|\boldsymbol{k}_0|}{h}\frac{1}{\sqrt{\lambda}},\\
\tau_{\sigma,1}^{-1} &= \rho_{\Lambda^{-1}}(\boldsymbol{\sigma}), & \tau_{\sigma,2}^{-1} &= \varepsilon,\\
\tau_{\nabla\alpha,1}^{-1} &= \sqrt{\lambda}|\nabla\alpha|, & \tau_{\nabla\alpha,2}^{-1} &= 0.
\end{aligned} \tag{4.22}$$

Now, we must specify an expression for the scaling parameter λ which, as we have seen, has the units of a velocity squared. A convenient choice is to take

$$\lambda = \frac{h^2}{|\boldsymbol{k}_0|^2\tau_{1,\mathrm{NS}}^2}, \tag{4.23}$$

where $\tau_{1,\mathrm{NS}}$ corresponds to the usual expression for τ_1 for the Navier-Stokes equations [10], so as to recover the expected expression for τ_1 at $\alpha \equiv 1$ (see (4.27) below). Note that, in the latter case, the contribution $\tau_{b,1}^{-1}$ becomes equal to the LHS of (4.14) which, if taken literally, leads to a nonsensical equation where τ_1 cancels out. This should be interpreted as meaning that this contribution *has the same asymptotic behavior* as the full τ_1. Therefore, it is superfluous to include it as its effect will be

absorbed in the algorithmic constants. In fact, neglecting the contribution to τ_1 of the mass conservation equation is also done in [11] using a different reasoning. For similar reasons, we will ignore the coefficient 4/3 in the expression of $\tau_{\nu,1}^{-1}$.

Furthermore, since α is assumed to be slowly varying over the element, it will be taken as a constant over each element and, in particular, we will take it to be equal to the maximum value it attains in it. Similarly, we will take the modulus of its gradient to be constant over the element and equal to its maximum value.

With these simplifications, the expression for the both stabilization parameters are given by

$$\tau_1 = \left(C_\alpha \tau_{1,\mathrm{NS}}^{-1} + \rho_{\Lambda^{-1}}(\boldsymbol{\sigma}) \right)^{-1}, \tag{4.24}$$

$$\tau_2 = \frac{h^2}{c_1 \alpha \tau_{1,\mathrm{NS}} + \varepsilon h^2}, \tag{4.25}$$

where

$$C_\alpha \coloneqq \alpha + \frac{h}{|\boldsymbol{k}_0|} |\nabla \alpha|, \tag{4.26}$$

$$\tau_{1,\mathrm{NS}} \coloneqq \left(c_1 \frac{\nu}{h^2} + c_2 \frac{|\boldsymbol{w}|}{h} \right)^{-1}, \tag{4.27}$$

and where $c_1 \coloneqq |\boldsymbol{k}_0|^2$, $c_2 \coloneqq |\boldsymbol{k}_0 \cos\phi|$, ϕ being the angle between $\boldsymbol{k}_0$ and $\boldsymbol{w}$, can be treated as numerical parameters (see, e.g., [10, 12]). Note that the expressions in (4.27) reduce to that corresponding to the stationary Navier-Stokes equations when $\alpha \equiv 1$ [10], which supports the choice made in defining the length scale λ. The second term in (4.25) is only strictly necessary for large of ε (see (5.10) below).

Moreover, note that the second term in the definition of C_α is in fact unnecessary if

$$\frac{h}{|\boldsymbol{k}_0|} |\nabla \alpha| \lesssim \frac{h}{|\boldsymbol{k}_0|} \frac{\alpha}{h} \sim \alpha. \tag{4.28}$$

That is, if the porosity changes are well resolved by the mesh. We will assume this to hold in the following, leaving issues related to steep porosity gradients to future work. We will therefore neglect the above-mentioned contribution in what follows.

It is not clear from the analysis above how one must evaluate the varying parameters $\alpha, \boldsymbol{w}$ since, given that we are solely interested in their asymptotic properties as the physical parameters take extreme values, it is only important that their values remain of the order of that of the varying fields they represent within each elemental domain. A common criterion is to evaluate the velocity modulus to its elemental maximum (a straightforward way to avoid setting it to zero when the velocity does not exactly vanish within the element). For simplicity, we will take this route in the theoretical considerations that follow, as well as evaluating α to its elemental minimum. However, while the optimization problem is trivial for some types of elements (e.g., linear elements), it can be cumbersome for others. Thus, in practice, the stabilization parameters can be taken as variable within the elements without altering their performance. This is what we have done in all the simulations presented.

5. Stability and convergence for the linearized problem and the ASGS method.

In this section we analyze the stabilization brought about by the method in a simplified

setting. The idea is to highlight why the generalization of the stabilization parameters given by (4.24) and (4.25) with respect to the case $\alpha \equiv 1$ (standard Navier-Stokes) still provides the necessary stability in the generic case. This stability is proved in a slightly weaker norm when $\alpha \neq 1$, although the numerical tests presented in section 7 indicate that, in practice, the accuracy of the method does not significantly deteriorate in this case.

We consider the ASGS algorithm with a uniform viscosity ν. For simplicity, we also consider $\boldsymbol{\sigma} = \sigma \mathbf{1}_3$ to be uniform. Under these conditions, and taking into account that we consider the porosity field well-resolved by the mesh in the sense of (4.28), we have

$$\tau_1 = \frac{1}{\alpha_K \tau_{1,\mathrm{NS}}^{-1} + \sigma}, \tag{5.1}$$

$$\tau_2 = \frac{h^2}{c_1 \alpha_K \tau_{1,\mathrm{NS}}}, \tag{5.2}$$

where α_K is some representative value of the porosity field within element K, such that $\alpha_{0,K} \leqslant \alpha_K \leqslant \alpha_{\infty,K}$, where we define $\alpha_{0,K} > 0$ and $\alpha_{\infty,K}$ to be the infimum and the supremum of $\alpha|_K$. As with the convective velocity norm in the definition of $\tau_{1,\mathrm{NS}}$, we will take $\alpha_K = \alpha_{\infty,K}$, which is also the natural choice according to the analysis presented below, as it yields to simplified estimates.

First, let us look at the stability of the Galerkin method for the linearized problem. Let us begin by expressing its associated bilinear form in terms of the velocity and pressure unknowns $\boldsymbol{u}_h$ and p_h as well as a given convective field $\boldsymbol{a}$:

$$\begin{aligned} B(\boldsymbol{a}, U_h, V_h) &= (\boldsymbol{v}_h \,,\, \alpha \boldsymbol{a} \cdot \nabla \boldsymbol{u}_h) + 2(\nabla \boldsymbol{v}_h \,,\, \alpha \nu \overset{\mathrm{DS}}{\Pi} \nabla \boldsymbol{u}_h) \\ &\quad + (\boldsymbol{v}_h \,,\, \alpha \nabla p_h) + (\boldsymbol{v}_h \,,\, \sigma \boldsymbol{u}_h) + (q_h \,,\, \varepsilon p_h) + (q_h \,,\, \nabla \cdot (\alpha \boldsymbol{u}_h)). \end{aligned} \tag{5.3}$$

Using the finite element unknown as the test function and assuming $\nabla \cdot (\alpha \boldsymbol{a}) = 0$ and $\boldsymbol{u}_h = \mathbf{0}$ on $\partial\Omega$, we obtain

$$B(\boldsymbol{a}, U_h, U_h) = 2\nu \left\| \alpha^{1/2} \overset{\mathrm{DS}}{\Pi} \nabla \boldsymbol{u}_h \right\|^2 + \left\| \sigma^{1/2} \boldsymbol{u}_h \right\|^2 + \varepsilon \|p_h\|^2, \tag{5.4}$$

which generalizes the stability estimate obtained for the Galerkin method for the standard Navier-Stokes equations. Note that, for very small viscosities or fluid volume fractions, the first term above will provide almost no control over the gradient of the velocity, leading to oscillations on the solution. This is what happens in the standard case, but here the problem is aggravated for small porosities.

Let us now study the stability of the stabilized bilinear form. We follow the analogous procedure to that in [10]:

$$\begin{aligned} B_{\mathrm{S}}(\boldsymbol{a}, U_h, U_h) &= B(\boldsymbol{a}, U_h, U_h) - \sum_K \langle \mathcal{L}^* V_h \,,\, \boldsymbol{\tau} \mathcal{L} U_h \rangle \\ &= 2\nu \left\| \alpha^{1/2} \overset{\mathrm{DS}}{\Pi} \nabla \boldsymbol{u}_h \right\|^2 + \left\| \sigma^{1/2} \boldsymbol{u}_h \right\|^2 + \varepsilon \|p_h\|^2 \\ &\quad + \left\| \tau_1^{1/2} \alpha X(U_h) \right\|_h^2 - \left\| \tau_1^{1/2} \big(2\nabla \cdot (\alpha \nu \overset{\mathrm{DS}}{\Pi} \nabla \boldsymbol{u}_h) - \sigma \boldsymbol{u}_h \big) \right\|_h^2 \\ &\quad + \left\| \tau_2^{1/2} \nabla \cdot (\alpha \boldsymbol{u}_h) \right\|_h^2 - \varepsilon^2 \left\| \tau_2^{1/2} p_h \right\|_h^2, \end{aligned} \tag{5.5}$$

where $\|\bullet\|_h := \sum_K \|\bullet\|_{L^2(K)}$ and $X(U_h) := \boldsymbol{a}\cdot\nabla\boldsymbol{u}_h + \nabla p_h$. Note that, strictly speaking, one has the term $\frac{1}{\alpha}\nabla\cdot(\alpha\boldsymbol{a})\boldsymbol{v}_h$ in the expansion of $\mathcal{L}^*V_h$. The inclusion of such term generates a number of crossed terms in (5.5) that actually harm stability. This could be solved by adding an analogous term on the original equation to reestablish that symmetry. By doing this, the strong form of the problem would not be changed, and one would have none of the undesirable crossed terms. This was the case analyzed in [10], where it is mentioned that such a formulation helps to make the problem well posed, especially for large values of ε. Here, we have opted for simplifying the formulation by removing the aforementioned term from $\mathcal{L}^*V_h$, leading to a simpler formulation with similar stability properties. Given that our focus is on small values of the compressibility, we do not miss out much in terms of the numerical advantages of the alternative formulation.

Let us bound the negative term in the second line of (5.5):

$$
\begin{aligned}
&-\left\|\tau_1^{1/2}\big(2\nabla\cdot(\alpha\nu\overset{\text{DS}}{\Pi}\nabla\boldsymbol{u}_h)-\sigma\boldsymbol{u}_h\big)\right\|_h^2\\
&=-\left\|\tau_1^{1/2}2\nabla\cdot(\alpha\nu\overset{\text{DS}}{\Pi}\nabla\boldsymbol{u}_h)\right\|_h^2-\left\|\tau_1^{1/2}\sigma\boldsymbol{u}_h\right\|_h^2\\
&\quad+2(\,2\tau_1\nabla\cdot\big(\nu\alpha\overset{\text{DS}}{\Pi}\nabla\boldsymbol{u}_h\big)\,,\sigma\boldsymbol{u}_h\,)_h\\
&\geqslant\sum_K\Big\{-4\frac{C_{\text{inv}}^2}{h^2}\nu^2\tau_1\alpha_K\left\|\alpha^{1/2}\overset{\text{DS}}{\Pi}\nabla\boldsymbol{u}_h\right\|_K^2-\tau_1\sigma^2\|\boldsymbol{u}_h\|_K^2\\
&\qquad-\frac{4}{\xi}\nu\sigma\tau_1\left\|\alpha^{1/2}\overset{\text{DS}}{\Pi}\nabla\boldsymbol{u}_h\right\|_K^2-\frac{\xi C_{\text{inv}}^2}{h^2}\nu\sigma\tau_1\alpha_K\|\boldsymbol{u}_h\|_K^2\Big\},
\end{aligned}
\tag{5.6}
$$

where the last two terms have been bounded by the term on the third line, as shown next:

$$
\begin{aligned}
&2(\,2\tau_1\nabla\cdot\big(\nu\alpha\overset{\text{DS}}{\Pi}\nabla\boldsymbol{u}_h\big)\,,\sigma\boldsymbol{u}_h\,)_h\\
&=2(\,2\nu^{1/2}\sigma^{1/2}\frac{\tau_1^{1/2}}{\alpha_K^{1/2}}\nabla\cdot\big(\alpha\overset{\text{DS}}{\Pi}\nabla\boldsymbol{u}_h\big)\,,\nu^{1/2}\alpha_K^{1/2}\tau_1^{1/2}\sigma^{1/2}\boldsymbol{u}_h\,)_h\\
&\geqslant-2\left\|2\nu^{1/2}\sigma^{1/2}\frac{\tau_1^{1/2}}{\alpha_K^{1/2}}\nabla\cdot\big(\alpha\overset{\text{DS}}{\Pi}\nabla\boldsymbol{u}_h\big)\right\|_h\left\|\nu^{1/2}\alpha_K^{1/2}\sigma^{1/2}\tau_1^{1/2}\boldsymbol{u}_h\right\|_h\\
&\geqslant-\frac{h^2}{\xi C_{\text{inv}}^2}\left\|2\nu^{1/2}\sigma^{1/2}\frac{\tau_1^{1/2}}{\alpha_K^{1/2}}\nabla\cdot\big(\alpha\overset{\text{DS}}{\Pi}\nabla\boldsymbol{u}_h\big)\right\|_h^2-\frac{\xi C_{\text{inv}}^2}{h^2}\left\|\nu^{1/2}\alpha_K^{1/2}\sigma^{1/2}\tau_1^{1/2}\boldsymbol{u}_h\right\|_h^2\\
&\geqslant\sum_K\Big\{-\frac{4}{\xi}\nu\sigma\tau_1\left\|\alpha^{1/2}\overset{\text{DS}}{\Pi}\nabla\boldsymbol{u}_h\right\|_K^2-\frac{\xi C_{\text{inv}}^2}{h^2}\nu\sigma\tau_1\alpha_K\|\boldsymbol{u}_h\|_K^2\Big\},
\end{aligned}
\tag{5.7}
$$

where we have used the inequality $-2xy\geqslant-\frac{1}{\xi}x^2-\xi y^2$, valid for any real numbers x,y,ξ, with $\xi>0$, as well as the following inverse estimate, which guarantees the existence of a constant C_{inv} independent of the mesh size such that

$$
\|\psi_h\|_{W_p^l(K)}\leqslant C_{\text{inv}}h^{l-m+d/p-d/q}\|\psi_h\|_{W_q^m(K)},
\tag{5.8}
$$

which is valid for $0 \leqslant m \leqslant l$ and $1 \leqslant p, q \leqslant \infty$ and any function ψ_h belonging to a finite-dimensional subspace of $H^l(K)$, under the assumption that the sequence of mesh refinements is non-degenerate (see, e.g., [4]).

Now, using (5.6) in (5.5) we obtain

$$
\begin{aligned}
B_{\mathrm{S}}(\boldsymbol{a}, U_h, U_h) \geqslant \sum_K \Big\{ & \varepsilon(1-\varepsilon\tau_2)\big\|p_h\big\|_K^2 \\
& + \nu\tau_1\left(\frac{2}{\tau_1} - 4C_{\mathrm{inv}}^2\alpha_K\frac{\nu}{h^2} - \frac{4}{\xi}\sigma\right)\Big\|\alpha^{1/2}\overset{\mathrm{DS}}{\Pi}\nabla\boldsymbol{u}_h\Big\|_K^2 \\
& + \sigma\tau_1\left(\frac{1}{\tau_1} - \sigma - \xi C_{\mathrm{inv}}^2\alpha_K\frac{\nu}{h^2}\right)\big\|\boldsymbol{u}_h\big\|_K^2 \\
& + \Big\|\tau_1^{1/2}\alpha X(U_h)\Big\|_K^2 + \Big\|\tau_2^{1/2}\nabla\cdot(\alpha\boldsymbol{u}_h)\Big\|_K^2\Big\}. \qquad (5.9)
\end{aligned}
$$

We have mentioned that ε must be small. In particular, we will require that

$$
\varepsilon < c_1 \inf_K \left\{\frac{\alpha_K^2\tau_{1,K}}{h^2}\right\}. \qquad (5.10)
$$

From (5.10), we have that the coefficient of the norm of the pressure term is

$$
\varepsilon(1-\varepsilon\tau_2) > C\varepsilon, \qquad (5.11)
$$

with $C > 0$, so as to make sure that the compressibility term does not switch, from adding, to removing stability. Using (4.24), the coefficient of $\big\|\alpha^{1/2}\overset{\mathrm{DS}}{\Pi}\nabla\boldsymbol{u}_h\big\|_K^2$ in (5.9) can be expanded into

$$
\nu\tau_1\left(\alpha_K\Big(2 - 4\frac{C_{\mathrm{inv}}^2}{c_1}\Big)\frac{c_1\nu}{h^2} + 2\alpha_K\frac{c_2|\boldsymbol{w}|_{\infty,K}}{h} + 2\Big(1-\frac{2}{\xi}\Big)\sigma\right) \geqslant C\nu, \qquad (5.12)
$$

if we take

$$
C = \min\left\{2 - 4\frac{C_{\mathrm{inv}}^2}{c_1},\ 2\Big(1-\frac{2}{\xi}\Big)\right\}. \qquad (5.13)
$$

On the other hand, the coefficient of $\big\|\boldsymbol{u}_h\big\|_K^2$ becomes

$$
\alpha_K\tau_1\sigma\left(\Big(1 - \frac{\xi C_{\mathrm{inv}}^2}{c_1}\Big)\frac{c_1\nu}{h^2} + \frac{c_2|\boldsymbol{w}|_{\infty,K}}{h}\right) \geqslant C\widetilde{\sigma}_\alpha, \qquad (5.14)
$$

where

$$
\widetilde{\sigma}_\alpha := \frac{\tau_{\mathrm{NS}}^{-1}\sigma}{\tau_{\mathrm{NS}}^{-1} + \sigma/\alpha_K}, \qquad (5.15)
$$

if we take

$$
C = 1 - \frac{\xi C_{\mathrm{inv}}^2}{c_1}. \qquad (5.16)
$$

In both cases it can be guaranteed that $C > 0$ by taking $\xi > 2$ if the condition

$$
c_1 > 2\xi C_{\mathrm{inv}}^2. \qquad (5.17)
$$

is met.

Remark 5.1. Condition (5.17) implies that the optimal value of c_1 depends on the element types involved through the inverse estimate constant. In particular, for elements of the same polynomial order k for the velocity and the pressure, taking $c_1 = 4k^4, c_2 = 2k^2$ turns out to be effective [14, 31], and was the choice made in all the numerical experiments presented below. This scaling is consistent with the quadratic dependence of C_{inv} on the polynomial order, which is known to grow as k^2 (see [14] for details). It is also consistent with the interpretation given above of c_1 as the square of the characteristic wave number of the oscillations produced by the *unresolved* part of the solution in terms of their contribution to $|\mathcal{L}U|^2_\Lambda$; see (4.4).

We have just shown that the following stability bound holds for the stabilized method:

LEMMA 5.2. *Assume that τ_1 is defined as in (4.24) and that $c_1 > 2\xi C_{inv}^2$, with $\xi > 2$. Then there exists a positive constant C such that for any $U_h = [\boldsymbol{u}_h; p_h] \in \mathcal{X}_h$ it holds that*

$$B_S(\boldsymbol{a}, U_h, U_h) \geqslant C|||U_h|||^2, \tag{5.18}$$

where

$$|||U_h||| := \left(\nu\left\|\alpha^{1/2}\overset{\text{DS}}{\Pi}\nabla\boldsymbol{u}_h\right\|^2 + \left\|\widetilde{\sigma}_\alpha^{1/2}\boldsymbol{u}_h\right\|^2 + \varepsilon\|p_h\|^2 + \left\|\tau_1^{1/2}\alpha X(U_h)\right\|_h^2 + \left\|\tau_2^{1/2}\nabla\cdot(\alpha\boldsymbol{u}_h)\right\|_h^2\right)^{1/2}, \tag{5.19}$$

with $\widetilde{\sigma}_\alpha$ given in (5.15).

Remark 5.3. Note that the quantity $\widetilde{\sigma}_\alpha$ differs from the quantity $\widetilde{\sigma}$ defined in [10] simply by the division of σ by α_K in the denominator. This seems to indicate a weaker control on $\boldsymbol{u}_h$ for large reaction terms when α_K is simultaneously very small. It turns out this not to be the case, as the asymptotic analysis presented below shows (see subsection 6.3) and the numerical tests corroborate.

It is also straightforward to follow an analogous process to that used in the proof of Lemma 2 in [10] to prove a certain continuity of the bilinear form B_{S}. In particular, it is possible to show that

LEMMA 5.4. *Assume that τ_1, τ_2 are defined as in (4.24) and (4.25) and that all the algorithmic constants involved are positive. Assume also that the field $\alpha\boldsymbol{a}$ is (weakly) divergence-free and $\nabla\alpha$ is uniformly bounded in Ω. Then, there exist a positive constant C, such that*

$$B_S(\boldsymbol{a}, U_h, U_h) \leqslant C\left(\left\|\frac{\tau_2^{1/2}}{h}\boldsymbol{u}_h\right\|_h + \left\|\frac{\tau_1^{1/2}}{h}p_h\right\|_h\right)|||V_h|||, \tag{5.20}$$

for all $U_h, V_h \in \mathcal{X}_h$.

Using Lemma 5.2 and the modified version of Lemma 5.4, and assuming that the solution of the linearized problem is sufficiently smooth, convergence follows as in [10]:

THEOREM 5.5. *Let U be the exact solution of the linearized problem corresponding to (3.21a), where $\boldsymbol{u}^{m-1}$ is replaced by a given $\boldsymbol{a}$ such that $\nabla\cdot(\alpha\boldsymbol{a}) = 0$ and where $\boldsymbol{\pi}_h^m = \boldsymbol{0}$ (ASGS method). Then, under the assumptions of Lemmas 5.2 and 5.4, there exists a positive constant C, such that*

$$|||E_h||| \leqslant C\sum_K \frac{1}{h_K}\left(\tau_{2,K}^{1/2}\text{E}_{\text{int},K}(\boldsymbol{u}) + \tau_{1,K}^{1/2}\text{E}_{\text{int},K}(p)\right), \tag{5.21}$$

where $E_h := U - U_h$ and where the interpolation error is defined as

$$\mathrm{E}_{\mathrm{int},K}(\psi) := h_K^{k_\psi+1} \|\psi\|_{H^{k_\psi+1}(K)}, \tag{5.22}$$

where ψ is the field being interpolated and k_ψ the corresponding polynomial order of the interpolation.

6. Robustness of the formulation with respect to changes in the physical parameters. Let us investigate how our convergence results are affected when the physical parameters take extreme values. We begin by writing down a dimensionless version of the momentum conservation equation:

$$Re\,\alpha^* \boldsymbol{u}^* \cdot \nabla^* \boldsymbol{u}^* - 2\nabla^* \cdot (\alpha^* \overset{\mathrm{DS}}{\Pi} \nabla^* \boldsymbol{u}^*) + (1 + Re + Da)\alpha^* \nabla^* p^* + Da\,\boldsymbol{u}^* = \boldsymbol{f}^*, \tag{6.1}$$

with

$$Re = \frac{UL}{\nu}, \quad Da = \frac{\sigma L^2}{\alpha_\infty \nu}, \tag{6.2}$$

where L, U, are the characteristic length and velocity scales, and $\alpha_\infty > 0$ is the supremum of the porosity field in the domain of interest. These scales are used in (6.1) to define the dimensionless counterparts of the various variables and differential operators: $\boldsymbol{u} = U\boldsymbol{u}^*$, $\alpha = \alpha_\infty \alpha^*$, $\nabla = L^{-1}\nabla^*$ and $\boldsymbol{f} = L^2/(\alpha_\infty \nu U)\boldsymbol{f}^*$. For the pressure, we have used a scaling that reflects our implicit assumption of the pressure gradient term being always of relevance. It is based on taking $p = Pp^*$, with

$$P = (1 + Re + Da)\frac{U\nu}{L}. \tag{6.3}$$

Clearly, such a scaling is not universally valid for all the solutions of (2.1) and (2.2) (e.g., at sufficiently low Reynolds numbers, one can pick the force term to achieve a null pressure field), but is valid in most flows of interest.

Equation (6.1) is particularly convenient for analyzing the relative weight of the various terms involved, given by their respective coefficients. In particular, we will study next the robustness of the convergence result (5.21) by considering different combinations of limiting values for Re and Da. For that, note the following asymptotic dependencies (as $h \to 0$):

$$\begin{aligned} \tau_1 &\sim \frac{1}{\alpha_K(1 + Re_h + Da_h)}\,\frac{h^2}{\nu}, \\ \tau_2 &\sim \frac{1 + Re_h}{\alpha_K}\,\nu, \\ \widetilde{\sigma}_\alpha &\sim \frac{(1 + Re_h)\,Da_h}{1 + Re_h + Da_h}\,\frac{\nu}{h^2}, \end{aligned} \tag{6.4}$$

where the h subindices refer to the fact that the element is considered the *domain of interest* (i.e., $L = h$).

6.1. Dominant viscous diffusion ($Re_h, Da_h \to 0$). In this case we have that

$$\tau_1 \sim \frac{h^2}{\alpha_K \nu},$$

$$\tau_2 \sim \frac{\nu}{\alpha_K},$$

$$\widetilde{\sigma}_{\alpha_K} \sim Da_h \frac{\nu}{h^2}.$$

With these estimates, (5.21) yields

$$\|\overset{\text{DS}}{\Pi}\nabla \boldsymbol{e}_u\| + \frac{1}{\nu}h\|\nabla e_p\|_h + \frac{1}{\alpha_0}\|\nabla\cdot(\alpha \boldsymbol{e}_u)\|_h \lesssim \frac{1}{\alpha_0}\left(\frac{\mathrm{E}_{\mathrm{int}}(\boldsymbol{u})}{h} + \frac{1}{\nu}\mathrm{E}_{\mathrm{int}}(p)\right). \tag{6.5}$$

Note that this result leads to the same drop in convergence order for the pressure as compared to the velocity that occurs in the conventional Navier-Stokes equations. The error is inversely proportional to α_0, so the estimate deteriorates as α_0 decreases, even though the third term on the LHS partially balances this deterioration. We will see that this linear drop in accuracy with decreasing minimal porosity is ubiquitous over the space of physical parameters. This is because the terms involving derivatives of the velocity are multiplied by the porosity in the continuous problem, which means that any inaccuracies in the velocity are weighted by the porosity, leading to (inversely proportional) larger errors in regions with smaller porosities. This is also manifested in the presence of α in the working norm of the problem.

It is interesting to examine what this result implies in terms of the control attained in practice for specific terms on the left-hand-side of (6.5). In particular, let us focus on the equal-order interpolation for the velocity and for the pressure, which is the case considered in the numerical experiments. Let U and P be the velocity and pressure characteristic values, such that $\mathrm{E}_{\mathrm{int}}(\boldsymbol{u}) = U\mathrm{E}^*_{\mathrm{int}}(\boldsymbol{u})$ and $\mathrm{E}_{\mathrm{int}}(p) = P\mathrm{E}^*_{\mathrm{int}}(p)$, where the asterisks denote dimensionless interpolation errors. Let us also define $\mathrm{E}^*_{\mathrm{int}} := \max\{\mathrm{E}^*_{\mathrm{int}}(\boldsymbol{u}), \mathrm{E}^*_{\mathrm{int}}(p)\}$.

In these conditions, and assuming that the scaling for the pressure given by (6.3) holds, (6.5) implies that

$$\|\overset{\text{DS}}{\Pi}\nabla \boldsymbol{e}_u\| \lesssim \frac{1}{\alpha_0}\left(1 + \frac{Ph}{U\nu}\right)\frac{\mathrm{E}_{\mathrm{int}}(\boldsymbol{u})}{h} \sim \frac{1}{\alpha_0}\left(1 + \frac{h}{L}\right)\frac{\mathrm{E}_{\mathrm{int}}(\boldsymbol{u})}{h} \sim \frac{1}{\alpha_0}\frac{\mathrm{E}_{\mathrm{int}}(\boldsymbol{u})}{h}, \tag{6.6}$$

where in the second estimate is obtained from $P \sim U\nu/L$ as $Re, Da \to 0$. This result is clearly optimal. Similarly, we have that

$$\|\nabla e_p\|_h \lesssim \frac{1}{\alpha_0}\left(\frac{U\nu}{h} + 1\right)\frac{\mathrm{E}_{\mathrm{int}}(p)}{h} \sim \frac{1}{\alpha_0}\left(\frac{L}{h} + 1\right)\frac{\mathrm{E}_{\mathrm{int}}(p)}{h}, \tag{6.7}$$

which shows why the pressure convergence rate will in general be one order below that of the velocity when viscosity is important.

6.2. Dominant convection ($Re_h \to \infty$).

In this case, we have the following estimates:

$$\tau_1 \sim \frac{h}{\alpha\|\boldsymbol{a}\|_{\infty,K}},$$

$$\tau_2 \sim \frac{h\|\boldsymbol{a}\|_{\infty,K}}{\alpha},$$

$$\widetilde{\sigma}_\alpha \sim Da_h \frac{\nu}{h^2},$$

from which (5.21) yields

$$\frac{1}{\|\boldsymbol{a}\|_\infty}\|\boldsymbol{a}\cdot\nabla \boldsymbol{e}_u + \nabla e_p\|_h + \|\nabla\cdot(\alpha \boldsymbol{e}_u)\|_h \lesssim \frac{1}{\alpha_0}\left(\frac{\mathrm{E}_{\mathrm{int}}(\boldsymbol{u})}{h} + \frac{1}{\|\boldsymbol{a}\|_\infty}\frac{\mathrm{E}_{\mathrm{int}}(p)}{h}\right), \tag{6.8}$$

where $\|\boldsymbol{a}\|_\infty$ is the supremum of $\|\boldsymbol{a}\|$ over Ω. Here again the error control is very similar to that one obtains for the regular Navier-Stokes equations as shown in [10]. For equal-order interpolations, we can use $P \sim U^2$ as $Re \to \infty$ to derive the following estimate:

$$\frac{1}{\|\boldsymbol{a}\|_\infty}\|\boldsymbol{a}\cdot\nabla\boldsymbol{e}_u + \nabla e_p\|_h \lesssim \frac{1}{\alpha_0}\left(U + \frac{P}{\|\boldsymbol{a}\|_\infty}\right)\frac{\mathrm{E}^*_{\mathrm{int}}}{h}, \tag{6.9}$$

which is optimal whenever the term $\boldsymbol{a}\cdot\nabla\boldsymbol{e}_u + \nabla e_p$ is of the same order as any of its two terms separately:

Dominant $\boldsymbol{a}\cdot\nabla\boldsymbol{e}_u$.

$$\|\frac{1}{\|\boldsymbol{a}\|_\infty}\boldsymbol{a}\cdot\nabla\boldsymbol{e}_u\|_h \lesssim \frac{1}{\alpha_0}\left(1 + \frac{U}{\|\boldsymbol{a}\|_\infty}\right)\frac{\mathrm{E}_{\mathrm{int}}(\boldsymbol{u})}{h} \sim \frac{1}{\alpha_0}\frac{\mathrm{E}_{\mathrm{int}}(\boldsymbol{u})}{h}. \tag{6.10}$$

Dominant ∇e_p.

$$\|\nabla e_p\|_h \lesssim \frac{1}{\alpha_0}\left(\frac{\|\boldsymbol{a}\|_\infty}{\sqrt{P}} + 1\right)\frac{\mathrm{E}_{\mathrm{int}}(p)}{h} \sim \frac{1}{\alpha_0}\frac{\mathrm{E}_{\mathrm{int}}(p)}{h}. \tag{6.11}$$

6.3. Dominant reaction ($Da_h \to \infty$).

The estimates for the numerical parameters are now as follows:

$$\tau_1 \sim \frac{\alpha}{\sigma},$$

$$\tau_2 \sim \frac{1 + Re_h}{\alpha}\nu,$$

$$\widetilde{\sigma}_\alpha \sim \alpha(1 + Re_h)\frac{\nu}{h^2}.$$

They yield the following error bound:

$$\begin{aligned}\|\overset{\mathrm{DS}}{\Pi}\nabla\boldsymbol{e}_u\| + (1 + Re_h)^{1/2}\frac{\|\boldsymbol{e}_u\|}{h} + \frac{\alpha_0}{\sigma^{1/2}\nu^{1/2}}\|\nabla e_p\|_h + \frac{(1 + Re_h)^{1/2}}{\alpha_0^{1/2}}\|\nabla\cdot(\alpha\boldsymbol{e}_u)\|_h,\\ \lesssim \frac{1}{\alpha_0}\left((1 + Re_h)^{1/2}\frac{\mathrm{E}_{\mathrm{int}}(\boldsymbol{u})}{h} + \frac{\alpha_0}{\sigma^{1/2}\nu^{1/2}}\frac{\mathrm{E}_{\mathrm{int}}(p)}{h}\right).\end{aligned}$$

Here the bound can again be considered optimal, even though the first term on the LHS will provide a more or less weak control, depending on the particular form of the $\overset{\mathrm{DS}}{\Pi}$ operator. Furthermore, note that the control on the pressure term deteriorates for very large Reynolds numbers, although this deterioration is slow, growing only with its square root. For equal-order discretizations, we can derive the following estimates:

$$\begin{aligned}\|\overset{\mathrm{DS}}{\Pi}\nabla\boldsymbol{e}_u\| &\lesssim \frac{1}{\alpha_0}\left((1 + Re_h)^{1/2} + \frac{\alpha_0}{\sigma^{1/2}\nu^{1/2}}\frac{P}{U}\right)\frac{\mathrm{E}_{\mathrm{int}}(\boldsymbol{u})}{h}\\ &\sim \left(\frac{1}{\alpha_0}(1 + Re_h)^{1/2} + \frac{Da^{1/2}}{\alpha_\infty^{1/2}}\right)\frac{\mathrm{E}_{\mathrm{int}}(\boldsymbol{u})}{h}.\end{aligned} \tag{6.12}$$

where we have used that $P \sim Da\,U\nu/h$ as $Da_h \to \infty$. It implies that the growth of either Re_h or Da could potentially undermine the optimality of the approximation of the gradient. Note however that the latter is the Damköhler number based on the macroscopic length L; that is, $Da = Da_h\,L^2/h^2$ and is thus is not expected

to be relevant except perhaps in extremely reaction-dominanted flows. The dependence of accuracy on the Reynolds number is similar to that of convection-dominated flows. These dependencies remain unaltered for $\alpha \equiv 1$. A similar reasoning leads to analogous estimates for $\|\boldsymbol{e}_u\|$.

Let us thus derive estimates for the norm of the gradient of the pressure. In this case, we have:

$$\|\nabla e_p\|_h \lesssim \frac{1}{\alpha_0}\left(\frac{(1+Re_h)^{1/2}}{\alpha_0}\, Da_h^{-1/2}\,\frac{L}{h}+1\right)\frac{\mathrm{E}_{\mathrm{int}}(p)}{h}. \tag{6.13}$$

Here the situation is reversed with respect to the dependence on Da_h. The loss of one order in the pressure accuracy is greatly mitigated by the presence of $Da_h^{-1/2}$ in reaction-dominated flows, except for the very finest meshes.

7. Numerical examples. We will resort to the method of manufactured solutions, deriving the exact expression for the forcing term that corresponds to the chosen velocity and pressure fields. We consider the unit square $(0,1)\times(0,1)$ as the fluid domain with null Dirichlet boundary conditions on all sides. Our pick for the fluid and pressure fields are

$$\begin{aligned}\boldsymbol{u}(x_1,x_2) &= U\frac{\alpha_0}{\alpha}\left(\sin(\pi x_1)\sin(\pi x_2)\boldsymbol{e}_1+\cos(\pi x_1)\cos(\pi x_2)\boldsymbol{e}_2\right),\\ p(x_1,x_2) &= P\cos(\pi x_1)\sin(\pi x_2),\end{aligned} \tag{7.1}$$

where $\boldsymbol{e}_i$ is the i-th coordinate basis vector and where U, P are the characteristic velocity and pressure scales that we take, as before, to be related by (6.3). The porosity field is defined in terms of the radial coordinate r, centered in the domain, as follows:

$$\alpha(r) = \begin{cases} \alpha_0 & r \leqslant r_1,\\ 1-\frac{1-\alpha_0}{1+\mathrm{e}^{\gamma(r)}} & r_1 < r < r_2,\\ 1 & r \geqslant r_2,\end{cases} \tag{7.2}$$

where $\gamma\colon (r_1,r_2)\to(-\infty,\infty)$ is a monotonically increasing function defined by

$$\gamma = \frac{2\eta-1}{\eta(1-\eta)}, \tag{7.3}$$

and

$$\eta := \frac{r^2-r_1^2}{r_2^2-r_1^2}, \tag{7.4}$$

where $0<r_1<r_2<1$. The formulas above define a smooth bump function with a central circular plateau where $\alpha=\alpha_0$ surrounded by the annular region defined by $r\in(r_1,r_2)$, on which the porosity monotonically increases with r up to $\alpha=1$ at $r=r_2$. Figure 1 shows $1-\alpha$, i.e., the matrix's volume fraction.

The objective of this example is to check the robustness of the empirical convergence rates obtained for the ASGS and OSGS formulations and to compare them to the analytical estimates derived in the previous sections. In particular, we will focus on the L^2-norm and the H^1-seminorm of the error, normalizing the velocity and pressure errors using their respective characteristic values U and P.

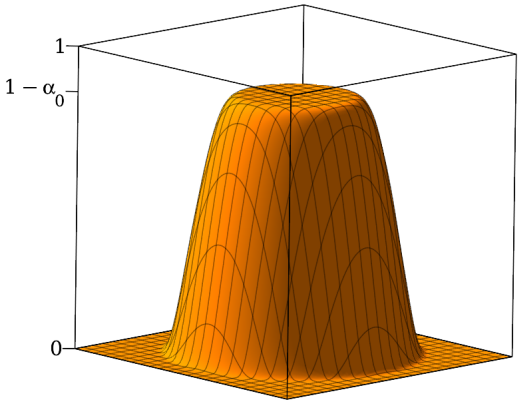

Fig. 1: Porous matrix's volume fraction field $1-\alpha$ used for manufactured tests.

In order to cover a wide range of regimes, we will consider all the combinations resulting from taking $Re, Da \in \{10^{-6}, 1, 10^{-6}\}$ and $\alpha_0 \in \{0.05, 0.5\}$. The large separation between the different values taken by Re and Da guarantees that the various flow regimes considered are approximately independent of the mesh refininement level. As the characteristic velocity and length scales are fixed, we vary the value of Re by changing the viscosity. The value of Da is varied through $\boldsymbol{\sigma}$. Doing so will allow us to analyse the performance of our formulation in the three limiting cases of interest, i.e., convection, diffusion and reaction-dominated flows.

For both 2D and 3D tests, we have considered the problem defined by (7.1). In the following subsections we present the particularities of the various simulations and the results obtained.

7.1. 2D cases.

We consider two types of elements: linear triangles ($\mathbb{P}_1$ elements) and biquadratic quadrilaterals ($\mathbb{Q}_2$ elements). The sequence of structured meshes is in both cases obtained by successively dividing the nodal distance by two, the coarsest one being given by a 10×10 grid, and the finest being 640×640. The triangle elements are obtained by dividing every resulting square into two triangles. In all the examples we take $\varepsilon = 0$.

Tables 1 and 2 contain the measured convergence rates for the L^2-norm and H^1-seminorm for the $\mathbb{P}_1$elements, along with the absolute errors in these norms measured on the finest mesh, i.e., the finest mesh error (FME). Tables 3 and 4 are the analogues for $\mathbb{Q}_2$ elements. Overall, let us note that there are no significant differences in accuracy between the ASGS and the OSGS methods over all the test cases. Furthermore, the results are compatible with the error estimates provided in section 6.

Indeed, one can immediately check that the effect of variations in the minimum porosity is consistent with the asymptotic analysis above. When when passing from $\alpha_0 = 0.5$ to $\alpha_0 = 0.05$ (even vs. odd-numbered lines in Tables 1 to 4), we observe a loss

in accuracy corresponding of around half an order of magnitude in terms of the FME. This tendency is quite robust although not without a few exceptions, particularly for the pressure when using linear elements.

For viscosity-dominated flows (rows 1-4, 7-8), the results are consistent with the predicted asymptotic bounds given by (6.6) and (6.7). Note that the FME values indicate that both the ASGS and OSGS methods show a very similar accuracy independently of the values taken by the physical parameters in this regime, except for the above-mentioned decrease in accuracy as α decreases. The predicted drop of one order in the pressure accuracy is observed in most cases for linear elements and is even more prevalent for biquadratic elements. The velocity error is optimal in call cases.

With respect to convection-dominated flows (cf. rows 5-6, 11-12, 17-18), we were unable to get the nonlinear iterations to converge with quadratic elements on the finest mesh when $\alpha = 0.5$, probably due to the stationary problem becoming ill-defined in this case. Such cases are identified in Tables 3 and 4 by the notation *n.c.* (not converged). For the remaining cases, the picture is very similar to that seen in the viscosity-dominanted regime: The predicted optimal asymptotic behavior is observed for the velocity and the pressure (which this time converges quadratically in all cases), as the estimates (6.10) and (6.11) suggest.

For reaction-dominated flows (rows 13-16), the analysis indicates a slightly more complex convergence profile. As a preamble, let us note the relation $Da = Da_h\, L^2/h^2$. The latter implies that the values of Da_h actually exhibit considerable variation accross the different meshes, becoming about 64 times smaller when passing from the coarses discretization to the finest one. In particular, we can estimate $Da_h \approx 10^6/80^2 \approx 150$ for the finest mesh, which could be considered marginally reaction-dominated. Nonetheless, note that the 3-order increase in $Da_h^{1/2}$ over the range that goes from 1 to 10^6 (compare rows 7-10 with rows 13-16) still leads to a quite robust decrease of the pressure error by a similar amount in the L^2-norm. For the H^1-norm, the decrease in error is smaller, although a consistent optimal-order (i.e., one order above the general case) convergence rate is only observed in the high-Da cases. These results are all consistent with (6.13). For the velocity error, the deterioration of its bound with Da suggested by (6.12) is not realised for linear elements (the FME barely grows when increasing $Da = 1$ to $Da = 10^6$ while leaving the other parameters unchanged). For biquadratic elements, a noticeble error growth is observed (compare, e.g., rows 9 and 15 in Tables 3 and 4), although still very far from the estimated $\sim Da^{1/2}$ effect.

7.2. 3D cases.

For the 3D examples, we use the z-wise extruded version of the same manufactured field. However, in order to break the symmetry, in this case we focus on unstructured meshes to make sure that the velocity vectors have a nonzero z-component due to the discretization errors. The domain is defined by a $(0,1)\times(0,1)\times(0,0.4)$ parallelepiped. Once again, the sequence of meshes is obtained by successively splitting the initial unstructured mesh sizes in two. In this case we consider only linear tetrahedra. The physical parameters are fixed to $(\alpha, Re, Da) = (0.5, 1, 1)$ for all the cases run.

The unstructured nature of the mesh makes it difficult to ensure that the boundary conditions imposed by the manufactured field are compatible with mass conservation in the discrete case, leading to an ill-posed problem. Thus, in this case we have resorted to the compressibility, taking $\varepsilon > 0$, which makes the problem well-posed. This also eliminates the indeterminancy in the pressure, removing the need to fix it

Table 1: Observed convergence rates and normalized finest mesh error (FME) for the 2D problem ($\mathbb{P}_1$ elements), calculated from the L^2-norm of the error obtained with the two finest meshes (theoretical convergence rates in parentheses)

velocity						
			slope (2)		FME	
Re	Da	α_0	ASGS	OSGS	ASGS	OSGS
10^{-6}	10^{-6}	0.5	2.00	2.00	8.48×10^{-6}	6.38×10^{-6}
10^{-6}	10^{-6}	0.05	2.00	2.00	2.95×10^{-5}	4.78×10^{-5}
1	10^{-6}	0.5	2.00	2.00	8.48×10^{-6}	6.38×10^{-6}
1	10^{-6}	0.05	2.00	2.00	2.95×10^{-5}	4.78×10^{-5}
10^6	10^{-6}	0.5	2.20	2.81	2.20×10^{-6}	2.22×10^{-6}
10^6	10^{-6}	0.05	2.07	2.08	1.10×10^{-5}	1.10×10^{-5}
10^{-6}	1	0.5	2.00	2.00	8.46×10^{-6}	6.31×10^{-6}
10^{-6}	1	0.05	2.00	2.00	2.90×10^{-5}	4.39×10^{-5}
1	1	0.5	2.00	2.00	8.46×10^{-6}	6.31×10^{-6}
1	1	0.05	2.00	2.00	2.90×10^{-5}	4.39×10^{-5}
10^6	1	0.5	2.20	2.81	2.20×10^{-6}	2.22×10^{-6}
10^6	1	0.05	2.07	2.08	1.10×10^{-5}	1.10×10^{-5}
10^{-6}	10^6	0.5	2.57	2.85	7.42×10^{-6}	1.94×10^{-5}
10^{-6}	10^6	0.05	2.11	2.83	2.20×10^{-5}	2.02×10^{-5}
1	10^6	0.5	2.57	2.85	7.42×10^{-6}	1.94×10^{-5}
1	10^6	0.05	2.11	2.83	2.19×10^{-5}	2.02×10^{-5}
10^6	10^6	0.5	2.60	2.56	2.60×10^{-6}	3.85×10^{-6}
10^6	10^6	0.05	2.08	2.11	7.44×10^{-6}	7.58×10^{-6}
pressure						
			slope (1)		FME	
Re	Da	α_0	ASGS	OSGS	ASGS	OSGS
10^{-6}	10^{-6}	0.5	1.00	1.83	1.30×10^{-2}	2.85×10^{-4}
10^{-6}	10^{-6}	0.05	1.55	2.00	1.61×10^{-3}	1.18×10^{-3}
1	10^{-6}	0.5	1.00	1.83	6.51×10^{-3}	1.43×10^{-4}
1	10^{-6}	0.05	1.55	2.00	8.04×10^{-4}	5.89×10^{-4}
10^6	10^{-6}	0.5	1.95	1.66	8.92×10^{-7}	1.07×10^{-6}
10^6	10^{-6}	0.05	2.02	2.03	1.51×10^{-6}	1.52×10^{-6}
10^{-6}	1	0.5	1.00	1.83	6.51×10^{-3}	1.42×10^{-4}
10^{-6}	1	0.05	1.55	2.00	8.05×10^{-4}	5.92×10^{-4}
1	1	0.5	1.00	1.83	4.34×10^{-3}	9.47×10^{-5}
1	1	0.05	1.55	2.00	5.37×10^{-4}	3.94×10^{-4}
10^6	1	0.5	1.95	1.66	8.92×10^{-7}	1.07×10^{-6}
10^6	1	0.05	2.02	2.03	1.51×10^{-6}	1.52×10^{-6}
10^{-6}	10^6	0.5	3.16	3.21	1.20×10^{-6}	1.22×10^{-6}
10^{-6}	10^6	0.05	2.95	2.97	1.98×10^{-6}	2.02×10^{-6}
1	10^6	0.5	3.16	3.21	1.20×10^{-6}	1.22×10^{-6}
1	10^6	0.05	2.95	2.97	1.98×10^{-6}	2.02×10^{-6}
10^6	10^6	0.5	1.89	1.66	6.26×10^{-7}	1.03×10^{-6}
10^6	10^6	0.05	2.03	2.05	1.33×10^{-6}	1.35×10^{-6}

Table 2: Observed convergence rates and normalized finest mesh error (FME) for the 2D problem ($\mathbb{P}_1$ elements), calculated from the H^1-seminorm of the error obtained with the two finest meshes (theoretical convergence rates in parentheses)

velocity						
			slope (1)		FME	
Re	Da	α_0	ASGS	OSGS	ASGS	OSGS
10^{-6}	10^{-6}	0.5	1.00	1.00	9.86×10^{-3}	9.86×10^{-3}
10^{-6}	10^{-6}	0.05	1.00	1.00	3.10×10^{-2}	3.10×10^{-2}
1	10^{-6}	0.5	1.00	1.00	9.86×10^{-3}	9.86×10^{-3}
1	10^{-6}	0.05	1.00	1.00	3.10×10^{-2}	3.10×10^{-2}
10^{6}	10^{-6}	0.5	1.02	1.09	9.88×10^{-3}	9.90×10^{-3}
10^{6}	10^{-6}	0.05	1.00	1.01	3.10×10^{-2}	3.11×10^{-2}
10^{-6}	1	0.5	1.00	1.00	9.86×10^{-3}	9.86×10^{-3}
10^{-6}	1	0.05	1.00	1.00	3.10×10^{-2}	3.10×10^{-2}
1	1	0.5	1.00	1.00	9.86×10^{-3}	9.86×10^{-3}
1	1	0.05	1.00	1.00	3.10×10^{-2}	3.10×10^{-2}
10^{6}	1	0.5	1.02	1.09	9.88×10^{-3}	9.90×10^{-3}
10^{6}	1	0.05	1.00	1.01	3.10×10^{-2}	3.11×10^{-2}
10^{-6}	10^{6}	0.5	1.00	1.82	9.86×10^{-3}	2.77×10^{-2}
10^{-6}	10^{6}	0.05	1.00	1.49	3.10×10^{-2}	4.06×10^{-2}
1	10^{6}	0.5	1.00	1.82	9.86×10^{-3}	2.77×10^{-2}
1	10^{6}	0.05	1.00	1.49	3.10×10^{-2}	4.06×10^{-2}
10^{6}	10^{6}	0.5	1.05	1.12	1.00×10^{-2}	1.07×10^{-2}
10^{6}	10^{6}	0.05	1.00	1.01	3.10×10^{-2}	3.11×10^{-2}
pressure						
			slope (-)		FME	
Re	Da	α_0	ASGS	OSGS	ASGS	OSGS
10^{-6}	10^{-6}	0.5	0.53	0.56	1.52×10^{-1}	2.88×10^{-1}
10^{-6}	10^{-6}	0.05	1.94	1.90	6.54×10^{-2}	7.02×10^{-2}
1	10^{-6}	0.5	0.53	0.57	7.61×10^{-2}	1.44×10^{-1}
1	10^{-6}	0.05	1.92	1.90	3.30×10^{-2}	3.53×10^{-2}
10^{6}	10^{-6}	0.5	1.00	1.00	5.45×10^{-3}	5.45×10^{-3}
10^{6}	10^{-6}	0.05	1.00	1.00	5.45×10^{-3}	5.45×10^{-3}
10^{-6}	1	0.5	0.53	0.57	7.61×10^{-2}	1.44×10^{-1}
10^{-6}	1	0.05	1.92	1.90	3.30×10^{-2}	3.55×10^{-2}
1	1	0.5	0.53	0.57	5.09×10^{-2}	9.56×10^{-2}
1	1	0.05	1.91	1.89	2.24×10^{-2}	2.40×10^{-2}
10^{6}	1	0.5	1.00	1.00	5.45×10^{-3}	5.45×10^{-3}
10^{6}	1	0.05	1.00	1.00	5.45×10^{-3}	5.45×10^{-3}
10^{-6}	10^{6}	0.5	1.00	1.00	5.45×10^{-3}	5.46×10^{-3}
10^{-6}	10^{6}	0.05	1.00	1.00	5.45×10^{-3}	5.46×10^{-3}
1	10^{6}	0.5	1.00	1.00	5.45×10^{-3}	5.46×10^{-3}
1	10^{6}	0.05	1.00	1.00	5.45×10^{-3}	5.46×10^{-3}
10^{6}	10^{6}	0.5	1.00	1.00	5.45×10^{-3}	5.45×10^{-3}
10^{6}	10^{6}	0.05	1.00	1.00	5.45×10^{-3}	5.45×10^{-3}

Table 3: Observed convergence rates and normalized finest mesh error (FME) for the 2D problem ($\mathbb{Q}_2$ elements), calculated from the L^2-norm of the error obtained with the two finest meshes (theoretical convergence rates in parentheses)

velocity						
			slope (3)		FME	
Re	Da	α_0	ASGS	OSGS	ASGS	OSGS
10^{-6}	10^{-6}	0.5	3.14	3.15	5.60×10^{-9}	5.60×10^{-9}
10^{-6}	10^{-6}	0.05	3.15	3.15	4.03×10^{-8}	4.03×10^{-8}
1	10^{-6}	0.5	3.14	3.15	5.60×10^{-9}	5.60×10^{-9}
1	10^{-6}	0.05	3.15	3.15	4.03×10^{-8}	4.03×10^{-8}
10^{6}	10^{-6}	0.5	n.c.	n.c.	n.c.	n.c.
10^{6}	10^{-6}	0.05	4.00	4.01	7.28×10^{-8}	7.27×10^{-8}
10^{-6}	1	0.5	3.14	3.15	5.60×10^{-9}	5.60×10^{-9}
10^{-6}	1	0.05	3.15	3.15	4.03×10^{-8}	4.03×10^{-8}
1	1	0.5	3.14	3.15	5.60×10^{-9}	5.60×10^{-9}
1	1	0.05	3.15	3.15	4.03×10^{-8}	4.03×10^{-8}
10^{6}	1	0.5	n.c.	n.c.	n.c.	n.c.
10^{6}	1	0.05	4.00	4.01	7.28×10^{-8}	7.27×10^{-8}
10^{-6}	10^{6}	0.5	3.86	4.10	4.89×10^{-8}	3.39×10^{-8}
10^{-6}	10^{6}	0.05	3.58	3.59	5.89×10^{-8}	5.13×10^{-8}
1	10^{6}	0.5	3.86	4.10	4.89×10^{-8}	3.39×10^{-8}
1	10^{6}	0.05	3.58	3.59	5.89×10^{-8}	5.13×10^{-8}
10^{6}	10^{6}	0.5	n.c.	n.c.	n.c.	n.c.
10^{6}	10^{6}	0.05	3.65	3.66	6.43×10^{-8}	6.44×10^{-8}
pressure						
			slope (2)		FME	
Re	Da	α_0	ASGS	OSGS	ASGS	OSGS
10^{-6}	10^{-6}	0.5	2.10	2.05	5.23×10^{-6}	5.18×10^{-5}
10^{-6}	10^{-6}	0.05	2.09	2.00	3.73×10^{-5}	3.66×10^{-3}
1	10^{-6}	0.5	2.10	2.05	2.61×10^{-6}	2.59×10^{-5}
1	10^{-6}	0.05	2.09	2.00	1.86×10^{-5}	1.83×10^{-4}
10^{6}	10^{-6}	0.5	n.c.	n.c.	n.c.	n.c.
10^{6}	10^{-6}	0.05	4.07	4.11	9.20×10^{-9}	9.24×10^{-9}
10^{-6}	1	0.5	2.10	2.05	2.61×10^{-6}	2.59×10^{-5}
10^{-6}	1	0.05	2.09	2.00	1.86×10^{-5}	1.83×10^{-4}
1	1	0.5	2.10	2.05	1.74×10^{-6}	1.73×10^{-5}
1	1	0.05	2.09	2.00	1.24×10^{-5}	1.22×10^{-4}
10^{6}	1	0.5	n.c.	n.c.	n.c.	n.c.
10^{6}	1	0.05	4.07	4.11	9.20×10^{-9}	9.24×10^{-9}
10^{-6}	10^{6}	0.5	3.10	2.92	5.63×10^{-10}	1.18×10^{-8}
10^{-6}	10^{6}	0.05	3.10	3.14	5.64×10^{-10}	1.02×10^{-9}
1	10^{6}	0.5	3.10	2.92	5.63×10^{-10}	1.18×10^{-8}
1	10^{6}	0.05	3.10	3.14	5.64×10^{-10}	1.02×10^{-9}
10^{6}	10^{6}	0.5	n.c.	n.c.	n.c.	n.c.
10^{6}	10^{6}	0.05	3.97	4.00	4.64×10^{-9}	4.65×10^{-9}

Table 4: Observed convergence rates and normalized finest mesh error (FME) for the 2D problem ($\mathbb{Q}_2$ elements), calculated from the H^1-seminorm of the error obtained with the two finest meshes (theoretical convergence rates in parentheses)

velocity						
			slope (2)		FME	
Re	Da	α_0	ASGS	OSGS	ASGS	OSGS
10^{-6}	10^{-6}	0.5	2.10	2.10	2.78×10^{-5}	2.78×10^{-5}
10^{-6}	10^{-6}	0.05	2.10	2.10	2.00×10^{-4}	2.00×10^{-4}
1	10^{-6}	0.5	2.10	2.10	2.78×10^{-5}	2.78×10^{-5}
1	10^{-6}	0.05	2.10	2.10	2.00×10^{-4}	2.00×10^{-4}
10^6	10^{-6}	0.5	n.c.	n.c.	n.c.	n.c.
10^6	10^{-6}	0.05	2.95	2.96	3.61×10^{-4}	3.61×10^{-4}
10^{-6}	1	0.5	2.10	2.10	2.78×10^{-5}	2.78×10^{-5}
10^{-6}	1	0.05	2.10	2.10	2.00×10^{-4}	2.00×10^{-4}
1	1	0.5	2.10	2.10	2.78×10^{-5}	2.78×10^{-5}
1	1	0.05	2.10	2.10	2.00×10^{-4}	2.00×10^{-4}
10^6	1	0.5	n.c.	n.c.	n.c.	n.c.
10^6	1	0.05	2.95	2.96	3.61×10^{-4}	3.61×10^{-4}
10^{-6}	10^6	0.5	2.81	3.05	2.13×10^{-4}	1.68×10^{-4}
10^{-6}	10^6	0.05	2.49	2.55	2.73×10^{-4}	2.54×10^{-4}
1	10^6	0.5	2.81	3.05	2.13×10^{-4}	1.68×10^{-4}
1	10^6	0.05	2.49	2.55	2.73×10^{-4}	2.54×10^{-4}
10^6	10^6	0.5	n.c.	n.c.	n.c.	n.c.
10^6	10^6	0.05	2.60	2.61	3.19×10^{-4}	3.19×10^{-4}
pressure						
			slope (1)		FME	
Re	Da	α_0	ASGS	OSGS	ASGS	OSGS
10^{-6}	10^{-6}	0.5	1.04	1.00	2.59×10^{-2}	2.56×10^{-2}
10^{-6}	10^{-6}	0.05	1.03	0.94	1.85×10^{-1}	1.81×10^{-1}
1	10^{-6}	0.5	1.04	1.00	1.29×10^{-2}	1.28×10^{-2}
1	10^{-6}	0.05	1.03	0.94	9.23×10^{-2}	9.05×10^{-2}
10^6	10^{-6}	0.5	n.c.	n.c.	n.c.	n.c.
10^6	10^{-6}	0.05	3.02	3.05	4.55×10^{-5}	4.57×10^{-5}
10^{-6}	1	0.5	1.04	1.00	1.29×10^{-2}	1.28×10^{-2}
10^{-6}	1	0.05	1.03	0.94	9.23×10^{-2}	9.06×10^{-2}
1	1	0.5	1.04	1.00	8.62×10^{-3}	8.53×10^{-3}
1	1	0.05	1.03	0.94	6.15×10^{-2}	6.04×10^{-2}
10^6	1	0.5	n.c.	n.c.	n.c.	n.c.
10^6	1	0.05	3.02	3.05	4.55×10^{-5}	4.57×10^{-5}
10^{-6}	10^6	0.5	2.10	2.10	2.00×10^{-6}	2.00×10^{-6}
10^{-6}	10^6	0.05	2.09	2.09	2.00×10^{-6}	2.00×10^{-6}
1	10^6	0.5	2.10	2.10	2.00×10^{-6}	2.00×10^{-6}
1	10^6	0.05	2.09	2.09	2.00×10^{-6}	2.00×10^{-6}
10^6	10^6	0.5	n.c.	n.c.	n.c.	n.c.
10^6	10^6	0.05	2.92	2.94	2.29×10^{-5}	2.29×10^{-5}

at one point (it imposes that the average pressure is zero, see [9]).

We make sure that condition (5.10) is met, by using the conservative value $\varepsilon = 0.0001\varepsilon_{\text{ref}}$, where

$$\varepsilon_{\text{ref}} := \frac{\alpha_0}{\nu(1 + Re + Da)} \leqslant \frac{\alpha_K}{\nu(1 + \frac{c_2}{c_1} Re_h + \frac{100}{c_1} Da_h)} \leqslant 100 \frac{c_1 \alpha_K^2 \tau_{1,K}}{h^2}, \tag{7.5}$$

where the first inequality holds for the parameter ranges chosen for the numerical experiments.

Additionally, we also add the previous value of the compressibility term to the right-hand side (i.e., we add εp^{n-1} to the right-hand side of **??**) at every nonlinear iteration. This *iterative penalty method*, anlyzed in [9], ensures that the manufactured solution is not altered.

Tables 5 and 6 list the results for the L^2-norm and H^1-seminorm. As in the 2D case, the results can be considered optimal, with very similar results for ASGS and OSGS.

Table 5: Observed convergence rates and normalized finest mesh error (FME) for the 3D problem, calculated from the L^2-norm of the error obtained with the two finest meshes (theoretical convergence rates in parentheses)

velocity				
	slope		FME	
element type	ASGS	OSGS	ASGS	OSGS
$\mathbb{P}_1$ (2)	2.01	2.07	3.27×10^{-4}	1.79×10^{-4}
$\mathbb{Q}_2$ (3)	3.18	3.22	8.20×10^{-5}	7.20×10^{-5}
pressure				
	slope		FME	
element type	ASGS	OSGS	ASGS	OSGS
$\mathbb{P}_1$ (1)	1.09	1.01	3.55×10^{-2}	4.13×10^{-2}
$\mathbb{Q}_2$ (2)	2.32	2.44	1.13×10^{-3}	2.37×10^{-3}

8. Conclusions. We have applied the VMS framework to generalize the formulation and analysis presented in [10] to the porous Navier-Stokes system, in such a way that the original method is recovered when $\alpha \equiv 1$. By using the abstract notation introduced in later works on VMS [15], we have strived to make it clearer to the less versed reader how the whole process is largely systematic once the particular equations are fit to the general framework.

Our analysis and numerical experiments show that the convergence properties of the original Navier-Stokes formulation are essentially preserved in the generalized setting. The analytical results have been corroborated in the numerical experiments, which show that the method remains just as robust in front of extreme variations in the physical parameters in the general case, as it is well-established to be for the original problem.

The specialization of the robustness analysis to equal-order polynomial elements presented in section 6 shows a few details previously not discussed, such as the mech-

Table 6: Observed convergence rates and normalized finest mesh error (FME) for the 3D problem, calculated from the H^1-seminorm of the error obtained with the two finest meshes (theoretical convergence rates in parentheses)

velocity				
	slope		FME	
element type	ASGS	OSGS	ASGS	OSGS
$\mathbb{P}_1$ (1)	1.04	1.03	6.15×10^{-2}	6.14×10^{-2}
$\mathbb{Q}_2$ (2)	2.02	2.10	1.31×10^{-2}	1.20×10^{-2}
pressure				
	slope		FME	
element type	ASGS	OSGS	ASGS	OSGS
$\mathbb{P}_1$ (-)	0.18	0.20	9.09×10^{-1}	5.14×10^{-1}
$\mathbb{Q}_2$ (1)	0.95	1.23	2.01×10^{-1}	3.67×10^{-1}

anism of pressure error improvement with growing Da_h or the (very weak in practice) deterioration of the velocity error with Da. By normalizing all the variables adequately, we have shown that the absolute errors are very stable with respect to changes in the physical parameters when the convergence rate is similar.

The abstract framework favored here makes it natural to include different particularizations of VMS in a very concise way. This has allowed us to implement both the ASGS and the OSGS versions of the method, showing through the many numerical experiments that both variants have very similar properties, at least for the problem considered.

There are several directions in which we think it is interesting to take the formulation developed here. First, we would like to study the possibility of simplifying the stabilized linear forms, given that not all the terms included are strictly necessary to obtain optimal convergence rates. In this sense, the so-called term-by-term stabilization approach [12] is a promising alternative.

Moreover, we are interested in studying the possibility of rewriting the formulation to make it suitable for large porosity gradients, including the possibility of considering discontinuous step-like changes, which have many engineering applications. As pointed out in [8], such formulations would likely require the integration by parts of the terms involving $\nabla\alpha$ in order to weaken the smoothness requirements of this field.

Another question not considered above is the effect of using the finite elements to interpolate the porosity field, as it would be natural to do in some applications. The error introduced by the interpolation can be treated similarly to quadrature error, but the simple convergence proof presented here would require cumbersome alterations due to the presence of α in the working norm of the problem, so we decided to leave this task for future work. Notwithstanding this, let us tentatively mention that our numerical experiments indicate that the model error introduced by the interpolation of α does not spoil the convergence properties of the method. For a work fully addressing this question, see [8].

Finally, we are also interested in the unsteady version of the equations, where α becomes a function of time too. This is the subject of current work.

Acknowledgments. The authors acknowledge the financial support from the CERCA programme of the Generalitat de Catalunya, and from the Spanish Ministry of Economy and Competitiveness, through the Severo Ochoa Centre of Excellence (2019-2023), under the grant CEX2018-000797-S, funded by MCIN/AEI/10.13039/501100011033.

Ramon Codina acknowledges the support received from the ICREA Acadèmia Research Program of the Catalan Government, Spain.

REFERENCES

[1] J.-L. Auriault, *On the domain of validity of brinkman's equation*, Transport in porous media, 79 (2009), pp. 215–223.

[2] S. Badia and R. Codina, *Stabilized continuous and discontinuous galerkin techniques for darcy flow*, Computer Methods in Applied Mechanics and Engineering, 199 (2010), pp. 1654–1667.

[3] J. Bear and Y. Bachmat, *Introduction to modeling of transport phenomena in porous media*, vol. 4, Springer Science & Business Media, 2012.

[4] S. C. Brenner, *The mathematical theory of finite element methods*, Springer, 2008.

[5] C. Calvo-Jurado, J. Casado-Díaz, and M. Luna-Laynez, *A brinkman law in the homogenization of the stationary navier–stokes system in a non-periodic porous medium*, Journal of Computational and Applied Mathematics, 354 (2019), pp. 191–197.

[6] C. Calvo-Jurado, J. Casado-Díaz, and M. Luna-Laynez, *A justification of the darcy law for a suspension of not self-similar solid particles non-periodically distributed*, Journal of Computational and Applied Mathematics, 404 (2022), p. 113415.

[7] Z. Chen, S. L. Lyons, and G. Qin, *Derivation of the forchheimer law via homogenization*, Transport in porous media, 44 (2001), pp. 325–335.

[8] P.-H. Cocquet, M. Rakotobe, D. Ramalingom, and A. Bastide, *Error analysis for the finite element approximation of the darcy–brinkman–forchheimer model for porous media with mixed boundary conditions*, Journal of Computational and Applied Mathematics, 381 (2021), p. 113008.

[9] R. Codina, *An iterative penalty method for the finite element solution of the stationary navier-stokes equations*, Computer methods in applied mechanics and engineering, 110 (1993), pp. 237–262.

[10] R. Codina, *A stabilized finite element method for generalized stationary incompressible flows*, Computer methods in applied mechanics and engineering, 190 (2001), pp. 2681–2706.

[11] R. Codina, *Stabilized finite element approximation of transient incompressible flows using orthogonal subscales*, Computer methods in applied mechanics and engineering, 191 (2002), pp. 4295–4321.

[12] R. Codina, *Analysis of a stabilized finite element approximation of the oseen equations using orthogonal subscales*, Applied Numerical Mathematics, 58 (2008), pp. 264–283.

[13] R. Codina, *Finite element approximation of the hyperbolic wave equation in mixed form*, Computer Methods in Applied Mechanics and Engineering, 197 (2008), pp. 1305–1322, https://api.semanticscholar.org/CorpusID:121409544.

[14] R. Codina, *On hp convergence of stabilized finite element methods for the convection–diffusion equation*, SeMA Journal, 75 (2018), pp. 591–606.

[15] R. Codina, S. Badia, J. Baiges, and J. Principe, *Variational multiscale methods in computational fluid dynamics*, Encyclopedia of Computational Mechanics Second Edition, (2018), pp. 1–28.

[16] R. Codina and O. Soto, *Approximation of the incompressible navier-stokes equations using orthogonal subscale stabilization and pressure segregation on anisotropic finite element meshes*, Computer Methods in Applied Mechanics and Engineering, 193 (2004), pp. 1403–1419, https://api.semanticscholar.org/CorpusID:120964013.

[17] A. Grillo, M. Carfagnay, and S. Federicoz, *The darcy-forchheimer law for modelling fluid flow in biological tissues*, Theoretical and Applied Mechanics, 41 (2014), pp. 283–322.

[18] M. Hamdan, *Single-phase flow through porous channels a review of flow models and channel entry conditions*, Applied Mathematics and Computation, 62 (1994), pp. 203–222, https://api.semanticscholar.org/CorpusID:120959384.

[19] U. Hornung, *Homogenization and porous media*, vol. 6, Springer Science & Business Media, 1997.

[20] T. J. Hughes and G. Sangalli, *Variational multiscale analysis: the fine-scale green's function, projection, optimization, localization, and stabilized methods*, SIAM Journal on Numerical

Analysis, 45 (2007), pp. 539–557.
[21] T. J. R. Hughes, G. Feijoo, L. Mazzei, and J. B. Quincy, *The variational multiscale method—a paradigm for computational mechanics*, Computer Methods in Applied Mechanics and Engineering, 166 (1998), pp. 3–24, https://api.semanticscholar.org/CorpusID:123229877.
[22] L. B. A. Nillama, J. Yang, and L. Yang, *An explicit stabilised finite element method for navier-stokes-brinkman equations*, Journal of Computational Physics, 457 (2022), p. 111033.
[23] H. R. Norouzi, R. Zarghami, R. Sotudeh-Gharebagh, and N. Mostoufi, *Coupled CFD-DEM modeling: formulation, implementation and application to multiphase flows*, John Wiley & Sons, 2016.
[24] A. Prosperetti and G. Tryggvason, *Computational methods for multiphase flow*, Cambridge university press, 2009.
[25] A. Quarteroni and S. Quarteroni, *Numerical models for differential problems*, vol. 2, Springer, 2009.
[26] C. A. B. Roa, J. Baiges, and R. Codina, *Variational multi-scale finite element approximation of the compressible navier-stokes equations*, International Journal of Numerical Methods for Heat & Fluid Flow, 26 (2016), pp. 1240–1271, https://api.semanticscholar.org/CorpusID:124907209.
[27] S. Shaw, P. Kameswaran, M. Narayana, and P. Sibanda, *Bioconvection in a non-darcy porous medium saturated with a nanofluid and oxytactic micro-organisms*, International Journal of Biomathematics, 7 (2014), p. 1450005.
[28] P. Skrzypacz, *Local projection stabilization for linearized brinkman-forchheimer-darcy equation*, AIP Conference Proceedings, 1880 (2017), p. 060010.
[29] M. Smith, A. Bale, L. Britt, L. Cunningham, J. Jones, H. Klein, and R. Wiley, *An investigation of non-darcy flow effects on hydraulic fractured oil and gas well performance*, in SPE Annual Technical Conference and Exhibition?, SPE, 2004, pp. SPE–90864.
[30] P. Verboven, D. Flick, B. Nicolaï, and G. Alvarez, *Modelling transport phenomena in refrigerated food bulks, packages and stacks: basics and advances*, International journal of refrigeration, 29 (2006), pp. 985–997.
[31] Á. P. Villota Cadena and R. Codina, *Aproximación de la ecuación escalar de convección-difusión-reacción con formulaciones estabilizadas de elementos finitos de alto orden*, Revista internacional de métodos numéricos para cálculo y diseño en ingeniería, 35 (2019), pp. 1–29.
[32] M. C. Vincent, C. M. Pearson, and J. Kullman, *Non-darcy and multiphase flow in propped fractures: case studies illustrate the dramatic effect on well productivity*, in SPE Western Regional Meeting, SPE, 1999, pp. SPE–54630.